Boundary Identification in the Domain of a Parabolic Partial Differential Equation

Tom P. Fredman

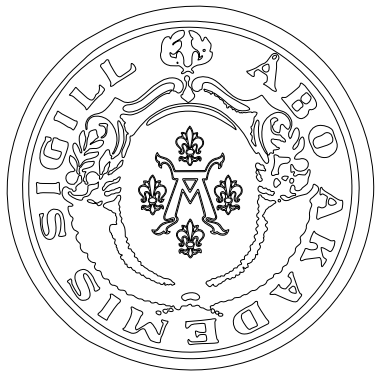

Department of Mathematics
Åbo Akademi University

Åbo, Finland 2008

ISBN 978-952-12-2218-4

Painosalama Oy
Åbo 2008

Preface

The greater part of this work was carried out at the Department of Mathematics at Åbo Akademi University during the years 2002-2008.

I wish to express my gratitude to my supervisor, Professor Olof Staffans for his guidance, encouragement and patience during the work. I also want to thank the official referees, Professor Kurt Bryan of Rose-Hulman Institute of Technology, Terre Haute and Professor Markku Nihtilä at University of Kuopio for their thorough review of and valuable comments on the manuscript.

In the course of the work, I have had the pleasure and benefit of sharing my thoughts and ideas with the staff at the Department of Mathematics and Heat Engineering Laboratory at Åbo Akademi University. Special thanks for encouragement and guidance go to Professor Hannu Toivonen of the Process Control Laboratory at Åbo Akademi University and Senior Lecturer Jockum Aniansson at the Royal Institute of Technology, Stockholm.

Finally, I would like to thank my family, particularly my wife Ulla, for their understanding and patience.

Björneborg, November 2008

Tom Fredman

Abstract

The background and inspiration for this study is previous work with applications of boundary identification in the metals processing industry. With an efficient boundary identification method, safety margins can be narrowed and maintenance intervals extended for high-temperature industrial equipment, without increasing the risk of failure and/or casualties. Ideally, such a method would be based on monitoring some indirectly influenced variable which is routinely measured or can be measured at a low cost. Furnace wall temperature at different positions is such a variable, suitable as input for a boundary identification method assessing the instantaneous lining wall thickness of the furnace.

We give a background and motivation for the choice of a spatially one-dimensional dynamical model for the boundary, i.e., a thickness description, by briefly considering the limitations of spatially two-dimensional models. Dynamics being more important for our applications than adding a spatial dimension and the advantages of the simplest formulation in possible industrial use made us choose the model formulation described in the latter parts of this work.

The sideways heat equation is a related topic with many characteristics carrying over to boundary identification, which is why we considered solution properties, noise contamination, regularization and ill-posedness more generally for the sideways heat equation.

For boundary identification we study a set of three different methods of estimating the boundary position, of which the two first ones have been developed from a purely mathematical standpoint and the third one from a more applied background. These methods have different characteristics with benefits and disadvantages. For the purely mathematically based methods we observed good accuracy and low computation cost, however, with low flexibility for dealing with nonlinear coefficients in the governing partial differential equation (PDE). For the third, more applied method, accuracy suffered from the ill-posedness of the more flexible formulation allowing (at least in principle) nonlinear and discontinuous coefficients in the governing PDE. Finally, we attempted to derive an error estimate, which was observed to conform with our experience from computational trials with the method.

We consider the present study as a good starting point and a mathematical basis for developing industrial applications of boundary identification, particularly toward dealing with real, nonlinear and discontinuous, material properties and sudden changes due to material "fall-off". With the methods outlined here, it seems feasible to obtain a robust, rapid and sufficiently accurate method using a reasonable amount of mathematical machinery.

Sammandrag - Abstract in Swedish

Bakgrunden och inspirationen till föreliggande studie är tidigare forskning i tillämpningar på randidentifiering i metallindustrin. Effektiv randidentifiering möjliggör mindre säkerhetsmarginaler och längre serviceintervall för apparaturen i industriella högtemperaturprocesser, utan ökad risk för materielhaverier. I idealfallet vore en metod för randidentifiering baserad på uppföljning av någon indirekt variabel som kan mätas rutinmässigt eller till en ringa kostnad. En dylik variabel för smältugnar är temperaturen i olika positioner i väggen. Denna kan utnyttjas som insignal till en randidentifieringsmetod för att övervaka ugnens väggtjocklek.

Vi ger en bakgrund och motivering till valet av den geometriskt endimensionella dynamiska modellen för randidentifiering, som diskuteras i arbetets senare del, framom en flerdimensionell geometrisk beskrivning. I de aktuella industriella tillämpningarna är dynamiken samt fördelarna med en enkel modellstruktur viktigare än exakt geometrisk beskrivning.

Lösningsmetoder för den s.k. sidledes värmeledningsekvationen har många saker gemensamt med randidentifiering. Därför studerar vi egenskaper hos lösningarna till denna ekvation, inverkan av mätfel och något som brukar kallas förorening av mätbrus, regularisering och allmännare följder av icke-välställdheten hos sidledes värmeledningsekvationen.

Vi studerar en uppsättning av tre olika metoder för randidentifiering, av vilka de två första är utvecklade från en strikt matematisk och den tredje från en mera tillämpad utgångspunkt. Metoderna har olika egenskaper med specifika fördelar och nackdelar. De rent matematiskt baserade metoderna karakteriseras av god noggrannhet och låg numerisk kostnad, dock till priset av låg flexibilitet i formuleringen av den modellbeskrivande partiella differentialekvationen. Den tredje, mera tillämpade, metoden kännetecknas av en sämre noggrannhet förorsakad av en högre grad av icke-välställdhet hos den mera flexibla modellen. För denna gjordes även en ansats till feluppskattning, som senare kunde observeras överensstämma med praktiska beräkningar med metoden.

Studien kan anses vara en god startpunkt och matematisk bas för utveckling av industriella tillämpningar av randidentifiering, speciellt mot hantering av olinjära och diskontinuerliga materialegenskaper och plötsliga förändringar orsakade av “nedfallande” väggmaterial. Med de behandlade metoderna förefaller det möjligt att uppnå en robust, snabb och tillräckligt noggrann metod av begränsad komplexitet för randidentifiering.

Background Publications

This thesis has been inspired and influenced by the engineering application treated in the following publications, referred to in the text by their Roman numerals.

/**I**/ T. P. Fredman. Accretions in the Blast Furnace Stack - Background Factors. *Canadian Metallurgical Quarterly* 41(4), 2002, pp. 475-486.

/**II**/ T. P. Fredman. Accretions in the Blast Furnace Stack - Diagnosis, Modeling and Control. *Canadian Metallurgical Quarterly* 42(1), 2003.

/**III**/ T. P. Fredman. A Boundary Identification Method for an Inverse Heat Conduction Problem with an Application in Ironmaking. *Heat and Mass Transfer - Wärme und Stoffübertragung* 41, 2004, pp. 95-103. Published electronically 2004.

/**IV**/ T. P. Fredman. Accretion Layer Thickness in the Blast Furnace Stack. In *61st Ironmaking Conference Proceedings*, volume 61, Iron & Steel Society, 2002.

/**V**/ T. P. Fredman. A Direct Integration Approach to Accretion Layer Estimation in the Blast Furnace Stack. In *ISSTech 2003 Conference Proceedings*, Iron & Steel Society, 2003.

/**VI**/ T. P. Fredman. A Boundary Movement Identification Method for a Parabolic Partial Differential Equation. *The European Conference on Numerical Mathematics and Advanced Applications, Prague, Czech Republic.* August 2003.

/**VII**/ T. P. Fredman. Identification of Boundary Movement from Internal Measurements. *Moving Boundaries, Seventh International Conference on Computational Modelling of Free and Moving Boundary Problems, Santa Fe, NM, U.S.A.*. November 2003.

/**VIII**/ T. P. Fredman. Formation and Detection of Accretions in the Blast Furnace Stack - A Literature Review. *Report 2001-2, Heat Engineering Laboratory, Åbo Akademi University*, 2001.

/**IX**/ T. P. Fredman. Investigation of Accretion Formation in Blast Furnace Shaft, final report. *ECSC Steel RTD Programme, contract 7210-PR-199*, 2004.

Publications /**III**/, /**VI**/ and /**VII**/ are reprinted in the appendix.

Contents

CHAPTER 1

Introduction

In this thesis, computational issues relating to boundary identification in the domain of a certain parabolic partial differential equation are studied. The topic was inspired by an engineering problem brought forward in the metals processing industry, involving certain high-temperature processes where the furnaces used are subject to cyclic wear and deposition of solid material /**I**, **II**, **VIII**/. This means that their inner surfaces can be regarded as moving boundaries. These processes typically involve various chemical reactors or transfer vessels designed for handling molten base metals, like iron or steel. To do this safely, appropriate insulation between the molten metal and equipment structure has to be ensured at all times. Since practical and economical considerations prevent direct visual inspection of the insulation status, some indirect means of checking must be used. A property that is easy enough to measure in an industrial environment is temperature, particularly at outer positions in the insulation material that can be maintained at relatively low temperatures /**IX**/. This is where the computations described in this thesis enter the picture: these safe temperature measurements can be used for real-time quantitative estimation of the remaining insulation thickness. In mathematical terms this means that the parabolic partial differential equation (PDE) governing the diffusion of heat through the insulation material is solved "sideways" from the measured temperature to the known temperature of the molten metal. The distance progressed in the solution is equivalent to the material thickness, since the measurement position is known. Hence, the approach essentially involves identification of part of the boundary for the PDE when the position of the other part, with the field variable measured, is known.

Boundary identification, in the context considered here, is an example of an *inverse problem*. It is impossible to define precisely what such a problem is, partly as a consequence of the rapid expansion and diversification during recent decades of the scientific field studying these problems. One might put it like Isakov [**26**], who states that the inverse A of an inverse problem is well-posed. This means that the mathematical model A with the "cause" or input f and the "effect" or output g, connected through the equation $A(f) = g$, possesses *existence*, *uniqueness* and stability for g. This property of what usually is termed the *direct problem*, is known as Hadamard's characterization of well-posedness. An inverse problem that does not have these characteristics is called *ill-posed*, although there are cases when both the direct problem and the inverse problem are well-posed. Roughly speaking, there are two types of inverse problems. Let the model A be known and the output g observed, then one might be interested in what kind of input f produced this output. Alternatively, let both the input f and the output g be observed. Now, what model A produced this mapping? Since determining a mathematical model from scratch in this way is a formidable task in, e.g., an industrial environment, one

usually estimates a small number of parameter values in a known model structure. Thus, this type of inverse problem is closely related to *identification* in control engineering.

Mathematical methods for boundary identification based on time-dependent measurements can be divided into dynamic, one-dimensional methods and static, multidimensional methods. This is due to the fact that finding a dynamic multidimensional boundary evolution is an under-determined problem, as will be seen in an example below. In both of these categories, different approaches ranging from integral equation formulations to numerical solution of related Cauchy-problems and least-squares fitting of parameters in presumed boundary shapes have been used. To get an impression of the typical features of boundary identification problems, consider the following

EXAMPLE 1. (One-dimensional boundary identification problem) In this one-dimensional boundary identification problem, it is desired to find the function $s(t) > 0$, characterizing the spatial dimension of the domain of the parabolic partial differential equation

$$u_{xx}(x,t) = u_t(x,t) \ , \tag{1}$$

$$\begin{gathered} u(0,t) = 0 = u(s(t),t) \ , \\ u(x,0) = \sin\left(\tfrac{\pi x}{s(0)}\right) \ , \ 0 \le x \le s(0) = 1 \ , \\ u_x(0,t) = g(t) \ , \ t \ge 0 \ , \end{gathered} \tag{2}$$

where the subscript denotes partial differentiation with respect to the index variable. The function $g(t)$ represents the "measurement" for determining $s(t)$. If $s(t)$ would be known, then the new time variable $\tau = \int_0^t \frac{\mathrm{d}p}{s^2(p)}$ would transform (1, 2) to a classical boundary value problem with Dirichlet boundary conditions, having a unique solution. This can be inferred if we introduce a Hilbert space H and note that $\frac{\partial^2}{\partial x^2}$ is the generator of a contraction semigroup. Then, there is a unique solution $u \in C^1([0,\infty), H)$ since $u(x,0) \in \mathcal{D}\left(-\frac{\partial^2}{\partial x^2}\right)$. In the identification problem, the measurement $g(t)$ is sufficient for determining the boundary evolution $s(t)$ and if the relative change can be considered small, so that $\frac{s'(t)}{s(t)} \approx 0$, then the solution $u(x,t)$ of (1, 2) can be approximated by

$$u(x,t) \approx \sin\left(\frac{\pi x}{s(t)}\right) \mathrm{e}^{-\pi^2 \int_0^t \frac{\mathrm{d}p}{s^2(p)}} \ , \tag{3}$$

which can be checked by noting that

$$\begin{gathered} \frac{\partial}{\partial t}\left(\sin\left(\tfrac{\pi x}{s(t)}\right)\mathrm{e}^{-\pi^2 \int_0^t \frac{\mathrm{d}p}{s^2(p)}}\right) = \\ -\tfrac{\pi^2}{s^2(t)}\left(\sin\left(\tfrac{\pi x}{s(t)}\right) + \tfrac{x s'(t)}{\pi}\cos\left(\tfrac{\pi x}{s(t)}\right)\right)\mathrm{e}^{-\pi^2 \int_0^t \frac{\mathrm{d}p}{s^2(p)}} \ , \end{gathered} \tag{4}$$

so the approximate solution (3) satisfies (1, 2) for the assumption $\frac{s'(t)}{s(t)} \approx 0$. Combining the measurement condition (2) with (3) and differentiation with respect to time, presuming that $g(t)$ is continuously differentiable, we get

$$g'(t) = -\left(\frac{s'(t)}{s(t)} + \frac{\pi^2}{s^2(t)}\right)\frac{\pi}{s(t)}\mathrm{e}^{-\pi^2 \int_0^t \frac{\mathrm{d}p}{s^2(p)}} \approx -\frac{\pi^2}{s^2(t)} g(t) \ , \tag{5}$$

which gives us the sought function

$$s(t) = \pi\sqrt{-\frac{g(t)}{g'(t)}}\ . \tag{6}$$

Suppose now that we, instead of the true function $g(t)$, measure a "corrupted" function approximating $g(t)$, characterized by the small number $\delta > 0$ and the positive integer n

$$g_{n,\delta}(t) = g(t) + \delta \sin\left(\frac{nt}{\delta}\right)\ . \tag{7}$$

This approximation is continuously differentiable as well and we obtain

$$g'_{n,\delta}(t) = g'(t) + n\cos\left(\frac{nt}{\delta}\right)\ . \tag{8}$$

Denoting the differences $\Delta g(t) = g_{n,\delta}(t) - g(t)$, $\Delta g'(t) = g'_{n,\delta}(t) - g'(t)$ we can compute the corresponding variation in $\pi^2 s^{-2}(t)$ from (6)

$$\Delta(\pi^2 s^{-2}(t)) = \frac{\Delta g(t)g'(t) - g(t)\Delta g'(t)}{g(t)g_{n,\delta}(t)}\ . \tag{9}$$

If the uncorrupted measurement and its derivative are considered bounded, such that $g(t) < M$ and $g'(t) < N$, we can make the estimate

$$|\Delta(\pi^2 s^{-2}(t))| \geq \frac{|\Delta g(t)g'(t) - g(t)\Delta g'(t)|}{|g(t)|\,(|g(t)| + \delta)} > \frac{||\Delta g(t)||g'(t)| - |g(t)||\Delta g'(t)||}{M\,(M+\delta)}\ . \tag{10}$$

Noting that $|\Delta g(t)| = \delta|\sin\left(\frac{nt}{\delta}\right)|$ and that $|\Delta g'(t)| = n|\cos\left(\frac{nt}{\delta}\right)|$, resulting in $\sup_{t\geq 0}|\Delta g(t)| = \delta$ and $\sup_{t\geq 0}|\Delta g'(t)| = n$ we then obtain

$$\sup_{t\geq 0}|\Delta(\pi^2 s^{-2}(t))| > \frac{Mn - N\delta}{M(M+\delta)}\ . \tag{11}$$

This means that high frequency noise in the measurement makes the variation in the reciprocal of $s(t)$ and hence also the variation in the function itself blow up independently of how small the absolute error in $g(t)$ is, since $\sup_{t\geq 0}|\Delta(\pi^2 s^{-2}(t))|$ in (11) is unbounded for $\frac{n}{\delta} \uparrow \infty$. Consequently, the problem of determining the function $s(t) > 0$ in (1, 2) from "real" measurements containing noise is ill-posed as the amplification of high-frequency components in the data is catastrophic. The example illustrates an inherent feature of inverse problems, namely error growth due to *measurement noise amplification*, resulting from a strong damping of input data in the direct problem.

Another reason for amplification of measurement errors in ill-posed computations, not present in example 1, is due to *model approximation errors* e.g. when a differential equation is discretized and solved numerically. Typically, when the model approximation error is reduced, the error due to the propagation of data increases and conversely.

The mathematically focused literature on dynamic boundary identification in the domain of parabolic PDE is scarce, probably due to the above mentioned restriction to one geometrical dimension. An integral equation approach based on the solution to the adjoint PDE is used in **[50]**. Judging from the described computation examples, their numerical solution strategy

works well even if the initial assumption of a slowly varying boundary function $s(t)$ is violated. This assumption originates from what in the literature on inverse problems is referred to as the "method of mappings" and in this case means rewriting the boundary identification problem as a coefficient identification problem. Hence, the unknown function is transferred to a coefficient of the PDE by renormalizing the domain to the interval $\frac{x}{s(t)} \in [0, 1]$. Coefficient estimation problems for PDE, on the other hand, have a fairly mature literature; some early applicable results can be found in **[27, 9]** and some more recent in **[11]**. An alternative method, focused on industrial application, which will be further described in this thesis, is presented in /**III-VII**/.

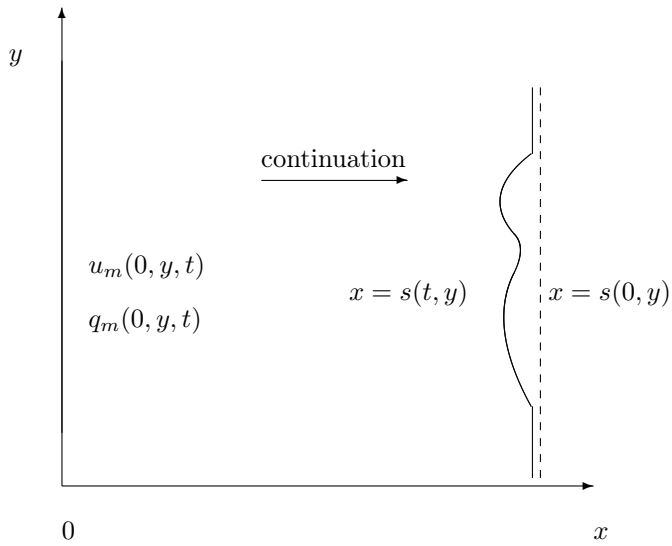

FIGURE 1.1. The two-dimensional dynamic boundary identification problem with Cauchy-data and two-dimensional time-varying boundary.

Identification of static two-dimensional boundaries in the domain of parabolic PDE is treated in a number of publications, thanks to the wide scope of related applications. Bryan and his co-workers **[5]** base their approach on a linearization of the relationship between the boundary profile and the solution of the PDE. From this a Fredholm integral equation of the first kind, containing the measurement data and surface profile function, can be derived and solved by a suitable numerical scheme. Uniqueness, stability and reconstruction properties relating to the strategy are also investigated in **[4, 6, 7]**. In a recent contribution, Bryan and Caudill **[8]** develop a Newton-like algorithm for solving the same problem, which leads to simple and efficient computations and regularization, as illustrated by computational examples. A limited number of contributions focused on industrial application of the technique can also be found in the literature: Skaar **[44]**, Sørli **[45]** and Radmoser **[41]** adopted a traditional optimization approach in fitting the solutions of the governing parabolic PDE for parametric boundary profiles to temperature data.

We opted for the one-dimensional dynamic boundary formulation, as the evolution of the boundary profile was judged more important than mapping a second spatial dimension. That capturing both the dynamics and the second dimension is infeasible we propose to show in

COUNTEREXAMPLE 1. (Two-dimensional dynamic boundary identification - Cauchy-data insufficient) Consider identification of the factorisable function $x = s(t, y) = f(t)g\left(\frac{y}{f(t)}\right)$ in

$$v_{xx}(x, y, t) + v_{yy}(x, y, t) = v_t(x, y, t) \ , \tag{12}$$

$$\begin{aligned} v(x, y, 0) &= h(x, y) \ , \\ v(0, y, t) &= u_m(0, y, t) \ , \\ v_x(0, y, t) &= q_m(0, y, t) \ , \\ v(s(t, y), y, t) &= v_s \ , \quad t \geq 0 \ , \end{aligned} \tag{13}$$

This problem, depicted in Figure 1.1, is essentially a continuation of the data on the y-axis to the boundary described by $x = s(t, y)$, having a known constant solution, i.e., $v(s(t, y), y, t) = v_s$. We claim, however, that the data is insufficient to obtain the function $s(t, y)$ and to see this, introduce the new independent variables $\eta = \frac{x}{f(t)}$, $\xi = \frac{y}{f(t)}$ resulting in $\eta = g(\xi)$. This will remove temporal dependence from the boundary and convert the problem to one with static domain.

In terms of the new independent variables the original problem can be written down for a new dependent variable $\vartheta(\eta, \xi, t) = v(f(t)\eta, f(t)\xi, t)$, satisfying the equation

$$\frac{f'(t)}{f(t)} \left(\eta \vartheta_\eta(\eta, \xi, t) + \xi \vartheta_\xi(\eta, \xi, t)\right) + \frac{1}{f^2(t)} \left(\vartheta_{\eta\eta}(\eta, \xi, t) + \vartheta_{\xi\xi}(\eta, \xi, t)\right) = \vartheta_t(\eta, y, t) \ , \tag{14}$$

$$\begin{aligned} \vartheta(\eta, \xi, 0) &= h(f(0)\eta, f(0)\xi) \ , \quad 0 \leq \eta \leq g(\xi) \ , \\ \vartheta(0, \xi, t) &= u_m(0, f(t)\xi, t) \ , \\ \vartheta_\eta(0, \xi, t) &= f(t) q_m(0, f(t)\xi, t) \ , \\ \vartheta(g(\xi), \xi, t) &= v_s \ , \quad t \geq 0 \ , \quad \xi \geq 0 \ . \end{aligned} \tag{15}$$

Now, (14, 15) lives on a fixed domain and we claim that *for an unknown, differentiable function $f(t)$, $g(\xi)$ may exist but it is not unique.* Support for this claim can be found in **[5]**, where uniqueness for the special case with $f'(t) = 0$, i.e. a static domain, is considered. There, the boundary was subject to a zero-flux condition as compared to the constant solution value in our case. However, if the function $f(t)$ is unknown, then the time-dependent coefficients in (14) as well as the temperature and flux data at $\eta = 0$ in (15) must be determined in the process of continuation. Hence, we have added more degrees of freedom to a formerly well-determined problem and the result is an under-determined problem. Thus, the given data does not determine $f(t)$ uniquely. The above argument makes it plausible that extracting general dynamics from the given Cauchy-data is impossible (although we do not prove this in detail). Consequently we proceed by restricting ourselves to one spatial and one temporal dimension, although it is possible that identifying a two-dimensional boundary would be feasible with some additional conditions on the solution **[6]**.

Another motivation for our choice of the "sideways formulation" of the solution over an integral equation approach is the flexibility and economy of our model. In various applications

the PDE is nonlinear due to solution-dependent coefficients arising from, e.g., thermal conductivity variation with temperature. Rewriting such a PDE into an integral equation would require restrictive approximations. In addition, any feasible integral equation must be solved numerically, so why not attack the original model formulation by a more direct numerical method instead of loosing information through intermediate approximation.

CHAPTER 2

The Sideways Heat Conduction Equation

The term "sideways heat conduction equation" was introduced in the eighties by Lars Eldén in a paper **[17]** on a remote temperature sensing problem, which is also frequently called the IHCP (Inverse Heat Conduction Problem). This remote temperature sensing task had been posed in ballistics, where it was desired to simulate heat conduction in the barrel of a cannon **[12]**. When a shell is fired by a cannon, there occurs sharp pulses in temperature and heat flux on the inner surface of the barrel, effectively ranging over some 20-30 milliseconds. Such rapid phenomena in an aggressive environment are not possible to monitor by conventional temperature sensing techniques, however the IHCP is an efficient and economical tool for their mathematical modeling.

We consider two related problems on the sideways heat conduction equation, of which the first in a semi-infinite geometry has wide application **[12, 37, 19]** as an approximation to the second finite geometry problem. The reason for this is that the semi-infinite geometry permits formulation as a simple Volterra integral equation, permitting versatile analysis and study of solution properties.

1. The quarter plane problem

The *quarter plane problem* is a diffusion problem in a semi-infinite geometry, where the objective is to compute $f(t) = u(0,t)$ when the solution, $g(t) = u(l,t)$, for a position $0 < l < \infty$ is known

$$u_{xx}(x,t) = u_t(x,t) \ , \tag{16}$$

$$\begin{gathered} u(l,t) = g(t) \ , \\ u(x,0) = 0 \ , \\ x \in [0,\infty), \quad t \in [0,\infty) \ , \end{gathered} \tag{17}$$

with the additional condition that the solution be bounded, $\lim_{x\to\infty} u(x,t) \leq u_\infty$.

1.1. Integral equation. The problem (16, 17) can be formulated **[12, 10]** as the Volterra integral equation of the first kind

$$(Kf)(t) = g(t) \ , \quad t \in [0,\infty) \ , \tag{18}$$

$$(Kf)(t) = \int_0^t k(l,t-\tau) f(\tau) \mathrm{d}\tau \ , \tag{19}$$

where the kernel is given by

$$k(l,t) = \frac{l}{2t^{3/2}\sqrt{\pi}} \mathrm{e}^{-\frac{l^2}{4t}} \ , \quad t > 0 \ , \quad k(l,0) = 0 \ . \tag{20}$$

2. The finite geometry problem

The corresponding *finite geometry problem* has the objective of computing the temperature $f(t) = v(0,t)$ at the remote end of a finite geometry in

$$v_{xx}(x,t) = v_t(x,t) \ , \tag{21}$$

$$\begin{gathered} v(l,t) = g(t) \ , \\ v_x(l,t) = h(t) \ , \\ v(x,0) = 0 \ , \\ x \in [0,l], \quad t \in [0,\infty) \ . \end{gathered} \tag{22}$$

Here, the requirement of boundedness in (16, 17) has been replaced by the measurement of the flux $v_x(l,t)$ at the accessible end of the geometry.

2.1. Integral equation. The problem (21, 22) can be formulated in integral equation form as well, with a different kernel function having similar mathematical properties as (20). Application of the theory in, e.g., chapters 4-6 of **[10]** leads to the representation

$$(Mf)(t) = h(t) + (Lg)(t) \ , \quad t \in [0,\infty) \ , \tag{23}$$

$$\begin{gathered} (Mf)(t) = \int_0^t \kappa(l, t-\tau) f(\tau) \mathrm{d}\tau \ , \\ (Lg)(t) = \int_0^t \kappa(0, t-\tau) g(\tau) \mathrm{d}\tau \ , \end{gathered} \tag{24}$$

where the kernel can be given, in terms of the kernel (20), by

$$\kappa(x,t) = \sum_{m=-\infty}^{\infty} \frac{\partial k(x+2m,t)}{\partial x} \ . \tag{25}$$

The integral equation (23) can be derived from the following theorem.

THEOREM 1. *(Existence and uniqueness) For piecewise-continuous f and g, the function*

$$v(x,t) = \int_0^t \vartheta(x, t-\tau) f(\tau) \mathrm{d}\tau - \int_0^t \vartheta(x-l, t-\tau) g(\tau) \mathrm{d}\tau \ , \tag{26}$$

where $\vartheta(x,t)$ is defined by

$$\vartheta(x,t) = \sum_{m=-\infty}^{\infty} k(x+2m,t) \ , \tag{27}$$

is the only bounded solution of (21, 22) regarded as a direct problem *with $f(t) = v(0,t)$ known.*

Proof. See Theorem 6.3.1. in Cannon **[10]**. □

In fact, Theorem 1 holds also for $f, g \in L_2(0,T)$. Proving this requires using certain tools from measure theory and specifying in what sense the derivatives of $v(x,t)$ exist. Moreover, the space of piecewise-continuous functions is dense in L_2 (see **[38]**, section D 12), so an arbitrary function in this space can be approximated to the desired accuracy by a piecewise-continuous function. Therefore, in what follows we will assume that any measurement data can be represented by piecewise-continuous functions.

REMARK 1. The kernel (25) is well-defined since the series (27) of continuous functions is uniformly convergent due to the fact that $k(x,t) \in C^\infty(\mathbb{R}^2)$ and

$$\begin{array}{c} \lim_{x\to 0^+} k(x,t) = 0 \ , \\ \lim_{t\to 0^+} k(x,t) = 0 \end{array} \tag{28}$$

and the limits on the other boundaries of the domain exist. Thus, $|k(x+2m,t)|$ as well as $\left|\frac{\partial k(x+2m,t)}{\partial x}\right|$ are bounded and Weierstrass M-test proves uniform convergence. Then, by Weierstrass M-test, also the series (25) converges uniformly and thus represents the spatial derivative of (27).

3. Fundamental solution properties

Solving the quarter plane as well as the finite geometry problem requires inversion of a smoothing Volterra integral operator, with essentially similar properties in both cases. Intuitively, if an operator acts smoothing in its domain, less desirable properties may be expected from the corresponding inverse operator, if it exists. We will start with the concept of smoothing and to what extent this relates to how ill-posed inverse problems can be considered.

3.1. Smoothing property and ill-posedness.

DEFINITION 1. (ν-smoothing property for a Volterra operator) The Volterra operator A, defined for by $f \in L_2(0,T)$ by

$$(Af)(t) := \int_0^t a(t,\tau) f(\tau) \mathrm{d}\tau \ , \quad \text{a. e. } t \in [0,T] \tag{29}$$

is ν-smoothing for integer $\nu \geq 1$ if the kernel a is such that $\frac{\partial^l a(t,t)}{\partial t^l} = 0$, for $t \in [0,T]$ and $l = 0, \ldots, \nu-2$ and $\frac{\partial^{\nu-1} a(t,t)}{\partial t^{\nu-1}} = 1$, for $t \in [0,T]$ with $\frac{\partial^\nu a}{\partial t^\nu}$ continuous on $[0,T]\times[0,T]$.

DEFINITION 2. (∞-smoothing for a Volterra operator) The Volterra operator A, of definition 1, is ∞-smoothing if $\frac{\partial^l a(t,t)}{\partial t^l} = 0$, for $t \in [0,T]$ and all $l = 0, 1, 2, \ldots$

LEMMA 1. *The integral operator K, (19), in the quarter plane problem and the integral operator M, (24), in the finite geometry problem are both ∞-smoothing.*

Proof. Observe that the kernel (20) is continuous for $t > 0$, $\lim_{t\to 0^+} k(\cdot,t) = 0$ so that $k(\cdot, t-t) = k(\cdot,0) = 0$. Furthermore, $\frac{\partial^l k(\cdot,0)}{\partial t^l} = 0$, for $l = 1, 2, \ldots$, since the derivative is proportional to a sum of terms of the form $t^{-n} k(\cdot,t)$. This means that definition 2 is fulfilled for both K, (19), and M, (24). □

The quarter plane problem (16, 17) is a classical example [**30**] of an ∞-smoothing problem and thus this inverse problem is severely ill-posed. Although the integral operator K in (19) can be inverted, its inverse is unbounded as seen from

LEMMA 2. *The integral operator K, (18), in the quarter plane problem, is a compact linear operator in $L_p(0,T)$, $1 \leq p \leq \infty$. The inverse operator K^{-1} exists on a densely defined subdomain of $L_p(0,T)$ and is unbounded.*

Proof. Adapted from [**12**]. Linearity is straightforward application of the Lebesque integral. Define the bounded, continuous function $q(t) \in L_1(\mathbb{R})$ in terms of the kernel (20) as

$$q(t) = \begin{cases} k(l,t)\ , & t > 0 \\ 0\ , & t \leq 0 \end{cases} . \tag{30}$$

Then, the Volterra integral equation (19) can be written as a Fredholm equation

$$(Kf)(t) = \int_0^T q(t-\tau) f(\tau) \mathrm{d}\tau\ . \tag{31}$$

The function $q(t,\tau) = q(t-\tau)$ is continuous on the square $0 \leq t,\ \tau \leq T$. Hence, K is a compact linear operator on $L_p(0,T)$, see [**28**] (p. 157). Since K is Volterra, its spectral radius is zero, see [**28**] (p. 154). We proceed to show that K is injective. Suppose $(Kf)(t) = 0$ almost everywhere on $[0,T]$ and extend $f(t)$ by zero for $\infty > t > T$. Then

$$\int_0^t q(t-\tau) f(\tau) \mathrm{d}\tau = 0 \quad \text{a.e.} \tag{32}$$

Laplace-transforming both sides leads to

$$\mathrm{e}^{-l\sqrt{\mathsf{p}}} F(\mathsf{p}) \equiv 0 \quad \text{a.e.}\ , \tag{33}$$

where $\sqrt{\mathsf{p}}$ is the principal square root of the complex variable p. Thus, $F(\mathsf{p}) \equiv 0$ implying $f(t) = 0$ almost everywhere on $0 \leq t < \infty$. In summary, $Kf = 0$ a. e. $\Rightarrow f = 0$ a. e. $\Leftrightarrow$ K is injective. The resolvent operator of the operator K is $R_\lambda(K) = (K - \lambda I)^{-1}$ [**29**]. Since the spectral radius of K is zero and $R_0(K)$ exists, the spectrum consists of the point $\{0\}$. Furthermore, $R_0(K)$ is defined on a set which is dense in $L_p(0,T)$, which means that per definition (in [**29**]) $R_0(K)$ and thus also K^{-1} must be unbounded on this set. □

For an unbounded time interval, compactness of the operator fails, but we still have the following result

LEMMA 3. *The integral operator K, (19), in the quarter plane problem, is a bounded injective linear operator in $L_p(0,\infty)$, $1 < p \leq \infty$. The inverse operator K^{-1}, defined on the range of K, exists and is unbounded.*

Proof. Linearity is straightforward. That K is bounded is shown in [**23**], section 2.2, Theorem 2.2, pp. 39-40 and 64. In the case $p = 2$, we have the following result: K is bounded iff its Laplace transform is bounded in the right half-plane, see [**46**] section A.3. Injectivity of K can be proved in the same way as in Lemma 2, without any need for the extension by zero of the function $f(t)$. For the unboundedness of the inverse, consider the following argument:

Assume that K^{-1}, defined on the range of K, is bounded. Then, for an $x \in L_p(0,\infty)$, $1 < p \leq \infty$, we have for norms in $L_p(0,\infty)$

$$\|x\| = \left\|K^{-1}Kx\right\| \leq L \|Kx\| \ . \tag{34}$$

Hence, if $\|x\| = 1$, we must have

$$\|Kx\| \geq \epsilon = \frac{1}{L} \ . \tag{35}$$

Consider now the function $\mathsf{f}(t) = 1$, $t \in [0,1]$ and $\mathsf{f}(t) = 0$ elsewhere. For the operator K, we have $k(l,\cdot) \in L_1(0,\infty)$ and $k(l,\cdot) \in L_p(0,\infty)$, $1 \leq p < \infty$. Let $\mathsf{f}_n(t) = n\mathsf{f}(nt)$, $t \in \mathbb{R}$. Then, according to Lemma 7.4. of section 2.7. in **[23]**, we have in $L_p(0,\infty)$, $1 \leq p < \infty$

$$\mathsf{f}_n * k(l,\cdot) = \int_0^t k(l,t-\tau)\mathsf{f}_n(\tau)\mathrm{d}\tau \to k(l,\cdot) \ , \quad n \to \infty \ . \tag{36}$$

In particular, according to Lemma 2.2. of section 2.2. in **[23]**, we have for $1 \leq p \leq \infty$ $\|\mathsf{f}_n * k(l,\cdot)\|_{L_p(0,\infty)} \leq \|k(l,\cdot)\|_{L_p(0,\infty)}$ (since $\|\mathsf{f}_n\|_{L_1(0,\infty)} = 1, \forall n$). We note that $\|\mathsf{f}_n\|_{L_\infty(0,\infty)} = n$ and compute the norm of f_n in $L_p(0,\infty)$, $1 \leq p < \infty$

$$\begin{array}{rcl} \left(\int_0^\infty |n\mathsf{f}(nt)|^p \,\mathrm{d}t\right)^{1/p} & = & n\left(\int_0^\infty |\mathsf{f}(y)|^p \,\frac{\mathrm{d}y}{n}\right)^{1/p} \\ & = & n^{1-1/p}\left(\int_0^1 \mathrm{d}y\right)^{1/p} \\ & = & n^{1-1/p} \ . \end{array} \tag{37}$$

Consider the sequence $\{x_n\}_{n=1}^\infty$, with

$$x_n(t) = \frac{\mathsf{f}_n(t)}{\|\mathsf{f}_n\|_{L_p(0,\infty)}} = \frac{n\mathsf{f}(nt)}{n^{1-1/p}} = n^{1/p}\mathsf{f}(nt) \ . \tag{38}$$

Thus, $\|x_n\|_{L_p(0,\infty)} = 1$ and for the sequence

$$\begin{array}{rcl} \|Kx_n\|_{L_p(0,\infty)} & = & \frac{1}{\|\mathsf{f}_n\|_{L_p(0,\infty)}} \|\mathsf{f}_n * k(l,\cdot)\|_{L_p(0,\infty)} \\ & \leq & \frac{1}{\|\mathsf{f}_n\|_{L_p(0,\infty)}} \|k(l,\cdot)\|_{L_p(0,\infty)} \\ & = & n^{1/p-1} \|k(l,\cdot)\|_{L_p(0,\infty)} \ . \end{array} \tag{39}$$

This leads us to the conclusion

$$\lim_{n\to\infty} \|Kx_n\| = 0 \ , \tag{40}$$

which means that no $\epsilon = \frac{1}{L} > 0$, defined in (35) can exist. Consequently, K^{-1} cannot be bounded. □

Although not proved here, the claim of Lemma 3 is true also for $p = 1$. Solution of the quarter plane problem essentially amounts to the application of K^{-1} to the data $g_m(t)$, corrupted by measurement errors. This is where the ill-posed nature of the problem manifests itself and things go wrong due to the unboundedness of K^{-1}. In other words, the mapping $g \mapsto f$ in (18) is not continuous. Consequently, some additional constraint on either the data or the solution is needed to proceed with the problem in a meaningful way.

To impose such a constraint, we will work in the Hilbert space $L_2(0,\infty)$, in order to use certain tools from Fourier analysis. We consider bounded measurement errors satisfying

$$\|g - g_m\|_{L_2(0,\infty)} \leq \varepsilon \ . \tag{41}$$

One way to take account of the unboundedness of K^{-1} is to apply an *a priori* bound on the solution, i.e.,

$$\|f\|_{L_2(0,\infty)} \leq M \ . \tag{42}$$

Under these two restrictions, (41 and 42), on the data it is possible to obtain stability for the solution of the quarter plane problem.

3.2. Hölder continuity. The quarter plane problem as well as the finite geometry problem are examples of ill-posed continuation problems in partial differential equations. As such, they can be stabilized in an appropriate Banach space by imposing an a priori bound on the solution **[15]**. This typically leads to a stability estimate of the logarithmic convexity type, which for the finite geometry problem, takes the form $\|v_1(x,\cdot) - v_2(x,\cdot)\| \leq 2M^{1-x/l}\varepsilon^{x/l}$, where v_1 and v_2 are any two continuations (solutions) and ε and M are defined through (41) and (42), respectively. This inequality was reported for the quarter plane problem in the landmark paper **[31]** and the proof for the finite geometry is similar. Carasso **[12]** considered an additional method for preventing blow-up of noise contained in the data. However, a problem with the stability estimate $\|v_1(x,\cdot) - v_2(x,\cdot)\| \leq 2M^{1-x/l}\varepsilon^{x/l}$ is that it does not tend to zero uniformly in x as $\varepsilon \downarrow 0$. Such *Hölder continuity* is not very useful in practice, considering instrumental levels of data error. In the limit $x \downarrow 0$ the stability result degenerates to the prior bound (42), a phenomenon termed *noise contamination* which is a characteristic of many stabilized ill-posed computations **[15]**.

We proceed with a proof of logarithmic convexity for the finite geometry problem via an auxiliary Lemma and the definition of a convex function **[43]**.

DEFINITION 3. A function $\mathcal{F}$ is convex on an interval $[0,l]$ if for any two points x_1 and x_2, $0 \leq x_1 \neq x_2 \leq l$ and any $0 \leq \lambda \leq 1$ the following inequality is satisfied

$$\mathcal{F}\left(\lambda x_1 + (1-\lambda)x_2\right) \leq \lambda\mathcal{F}(x_1) + (1-\lambda)\mathcal{F}(x_2) \ . \tag{43}$$

Recall first the standard result that a $C^2([0,l])$ function $\mathcal{F}$ is convex iff $\mathcal{F}'' \geq 0$. This implies that the function $\log\mathcal{F}$ is convex iff $\mathcal{F}\mathcal{F}'' - (\mathcal{F}')^2 \geq 0$ and we say that $\mathcal{F}$ is logarithmically convex or log convex. The following Lemma shows that log convexity implies $\mathcal{F} > 0$ and a certain inequality.

LEMMA 4. *Let $\mathcal{F} \in C([0,l])$ be log convex on its domain and $\lambda \in [0,1]$. Then, $\mathcal{F} > 0$ and*

$$\mathcal{F}\left(\lambda \cdot x_1 + (1-\lambda)\cdot x_2\right) \leq \mathcal{F}(x_1)^{\lambda}\mathcal{F}(x_2)^{(1-\lambda)} \ . \tag{44}$$

Proof. Since $\mathcal{F}$ is log convex, $\log\mathcal{F}$ exists and is convex, i.e., for $0 \leq x_1 \neq x_2 \leq l$, $0 \leq \lambda \leq 1$ we have $\mathcal{F} > 0$ and

$$\begin{gathered}\log\mathcal{F}\left(\lambda \cdot x_1 + (1-\lambda)\cdot x_2\right) \leq \lambda \cdot \log\mathcal{F}(x_1) + (1-\lambda)\cdot\log\mathcal{F}(x_2) \ \Leftrightarrow \\ \mathcal{F}\left(\lambda \cdot x_1 + (1-\lambda)\cdot x_2\right) \leq \mathcal{F}(x_1)^{\lambda}\mathcal{F}(x_2)^{(1-\lambda)} \ .\end{gathered} \tag{45}$$

□

THEOREM 2. *Let v_1 and v_2 be any two solutions of the problem (21) and (22) and let ε and M be defined through (41) and (42), respectively. Then*

$$\|v_1(x,\cdot) - v_2(x,\cdot)\| \leq 2M^{1-x/l}\varepsilon^{x/l} \tag{46}$$

Proof. Denote $\Delta v = v_1 - v_2$ and $\mathcal{F}(x) = \|\Delta v(x,\cdot)\|^2$. Then, Δv satisfies the differential equation (21). Taking Fourier transforms in (21) with respect to t, we see that the Fourier transform of Δv is given by

$$\widehat{\Delta v}(x,\omega) = \mathrm{e}^{\sqrt{i\omega}(l-x)}\widehat{\Delta v}(l,\omega)\ . \tag{47}$$

The Parseval relation gives

$$\mathcal{F}(x) = \int_{-\infty}^{\infty} |\widehat{\Delta v}(x,\omega)|^2 \mathrm{d}\omega = \int_{-\infty}^{\infty} \mathrm{e}^{\sqrt{2|\omega|}(l-x)} |\widehat{\Delta v}(l,\omega)|^2 \mathrm{d}\omega\ . \tag{48}$$

Hence,

$$\begin{gathered}\mathcal{F}(x)\mathcal{F}''(x) - (\mathcal{F}'(x))^2 = \left(\int_{-\infty}^{\infty} |\widehat{\Delta v}(x,\omega)|^2 \mathrm{d}\omega\right)\left(\int_{-\infty}^{\infty} 2|\omega||\widehat{\Delta v}(x,\omega)|^2 \mathrm{d}\omega\right) - \\ \left(\int_{-\infty}^{\infty} \sqrt{2|\omega|}|\widehat{\Delta v}(x,\omega)|^2 \mathrm{d}\omega\right)^2 \geq 0\ ,\end{gathered} \tag{49}$$

where the last relation follows from the Cauchy-Schwarz inequality. Consequently, $\mathcal{F}$ is log convex and has the property (44), with $x_1 = 0$, $x_2 = l$ and $\lambda = \frac{x}{l} \in [0,1]$, of Lemma 4

$$\|v_1(x,\cdot) - v_2(x,\cdot)\|^2 \leq \left(\|v_1(0,\cdot) - v_2(0,\cdot)\|^2\right)^{1-\frac{x}{l}} \left(\|v_1(l,\cdot) - v_2(l,\cdot)\|^2\right)^{\frac{x}{l}}\ . \tag{50}$$

The bound (42) leads to the inequality

$$\|v_1(0,\cdot) - v_2(0,\cdot)\| \leq \|v_1(0,\cdot)\| + \|v_2(0,\cdot)\| \leq 2M \tag{51}$$

and the boundary condition (22) together with (41) gives

$$\begin{gathered}\|v_1(l,\cdot) - v_2(l,\cdot)\| = \|v_1(l,\cdot) - g_m + g_m - v_2(l,\cdot)\| \leq \\ \|v_1(l,\cdot) - g_m\| + \|v_2(l,\cdot) - g_m\| = 2\varepsilon\ .\end{gathered} \tag{52}$$

If we insert the bounds (51) and (52) into (50), we obtain the desired result

$$\begin{gathered}\|v_1(x,\cdot) - v_2(x,\cdot)\| \leq \\ \|v_1(0,\cdot) - v_2(0,\cdot)\|^{1-\frac{x}{l}}\, \|v_1(l,\cdot) - v_2(l,\cdot)\|^{\frac{x}{l}} \leq 2M^{1-\frac{x}{l}}\varepsilon^{\frac{x}{l}}\ .\end{gathered} \tag{53}$$

□

REMARK 2. Hölder continuity (53) is an *intrinsic* characteristic found in solutions of both the quarter plane (16, 17) and the finite geometry problem (21, 22). In both of these cases, the proof above applies (with the addition of a stabilizing bound like (42) for the flux to the finite geometry problem). Since the flux in the latter case satisfies a differential equation and boundary conditions similar to (21, 22), Hölder continuity here also applies to the flux.

3.3. Improving Hölder continuity. Although an inherent feature of both the quarter plane and the finite geometry problem, Hölder continuity can be refined or "improved" if further constraints can be placed on the solution. Such constraints can be motivated, e.g., by the physics being modeled by the problem. Perhaps the least restrictive along these lines is the "Slow Evolution from the Continuation Boundary" (SECB) constraint recently introduced by Carasso. **[15, 16]** This means that the variation in the solution in the neighborhood of the boundary, where Hölder continuity causes the phenomenon of noise contamination, can be assumed to be small. In short, for the finite geometry problem, if the solution satisfies $\|v(x_0,\cdot) - v(0,\cdot)\| \le \mathcal{M}\varepsilon$ for a certain class of values for x_0, then there exists a constant $\Gamma(\mathcal{M}, x_0)$ such that $\|v_1(x,\cdot) - v_2(x,\cdot)\| \le 2\Gamma^{1-x/l}\varepsilon$, where v_1 and v_2 are any two continuations (solutions) and ε is defined through (41). Typically, this bound is superior to the Hölder continuity, since $\Gamma \ll M/\varepsilon$.

Following **[15, 16]**, we proceed with stability for the situation with valid SECB, starting with an auxiliary result.

LEMMA 5. *With given ε, M and $\mathcal{M}$ satisfying $0 < \varepsilon \ll M$ and $0 < \mathcal{M} \ll M/\varepsilon$, let*

$$x_0^*(\varepsilon, M, \mathcal{M}) = \frac{\log \frac{M}{M - \mathcal{M}\varepsilon}}{\log \frac{M}{\varepsilon}} \ . \tag{54}$$

For $x_0^* < x_0/l < 1$, let $\Gamma(\mathcal{M}, x_0)$ be the unique root of the transcendental equation

$$\mathtt{x} = \mathcal{M} + \mathtt{x}^{1-\frac{x_0}{l}} \ . \tag{55}$$

Then

$$\begin{aligned} &\mathcal{M} + 1 < \Gamma < \tfrac{M}{\varepsilon} \ , \\ &\tfrac{l\mathcal{M}}{x_0} \le \Gamma \log \Gamma \le \tfrac{l\mathcal{M}}{x_0} \cdot \tfrac{\Gamma}{\Gamma - \mathcal{M}} \ , \\ &\Gamma \log \Gamma \approx \tfrac{l\mathcal{M}}{x_0} \le \tfrac{l x_0^*}{x_0} \cdot \tfrac{M}{\varepsilon} \cdot \log \tfrac{M}{\varepsilon} \ , \quad \mathcal{M} \ll \Gamma \ . \end{aligned} \tag{56}$$

Furthermore, if $\mathcal{M}+1 \le x_{(0)} \le \frac{M}{\varepsilon}$, the iteration $\mathtt{x}_{(n+1)} = \mathcal{M} + \mathtt{x}_{(n)}^{1-\frac{x_0}{l}}$, $n = 0, 1, \ldots$, converges to Γ.

Proof. Existence of a unique root to (55) is seen from the fact that $\mathcal{M} > 0$ together with the linearity in x for the left hand side and sublinearity in x for the right hand side. From (54), we have $M/\varepsilon = \mathcal{M} + (M/\varepsilon)^{1-x_0^*}$, so M/ε solves (55) for $x_0/l = x_0^*$. The roots of (55) decrease monotonically with increasing x_0, which can be observed, e.g., by graphically comparing the left and right hand sides of (55). Thus $\Gamma < M/\varepsilon$ if $x_0/l > x_0^*$ and $\Gamma > 1$ and since the smallest root of (55) is obtained for $x_0/l = 1$, we obtain the bound $\Gamma > \mathcal{M} + 1$. This proves the first inequality of (56).

Using the known inequality $w \le \log \frac{1}{1-w} \le \frac{w}{1-w}$, $0 \le w < 1$, with $w = \frac{\mathcal{M}}{\Gamma}$ and keeping in mind that Γ solves (55), we find

$$\tfrac{\mathcal{M}}{\Gamma} \le \log \tfrac{\Gamma}{\Gamma - \mathcal{M}} = \tfrac{x_0}{l} \log \Gamma \le \tfrac{\mathcal{M}}{\Gamma - \mathcal{M}} \Leftrightarrow \tfrac{l\mathcal{M}}{x_0} \le \Gamma \log \Gamma \le \tfrac{\mathcal{M}}{1 - \frac{\mathcal{M}}{\Gamma}} \cdot \tfrac{l}{x_0} \ , \tag{57}$$

which proves the second inequality of (56) and the approximation if $\mathcal{M} \ll \Gamma$. Again, using the inequality above with $w = \frac{\mathcal{M}\varepsilon}{M}$ leads, using (54), to

$$\frac{\mathcal{M}\varepsilon}{M} \leq \log \frac{M}{M-\mathcal{M}\varepsilon} = x_0^* \log \frac{M}{\varepsilon} \Leftrightarrow \frac{l\mathcal{M}}{x_0} \leq \left(\frac{lx_0^*}{x_0}\right)\left(\frac{M}{\varepsilon}\right) \log \frac{M}{\varepsilon} \ , \tag{58}$$

which is the final inequality of (56). The statement of convergence for the iteration to a solution of (55) can be verified by application of a standard fixed point Theorem, **[29]** as the mapping $\mathtt{x} \mapsto \mathcal{M} + \mathtt{x}^{1-\frac{x_0}{l}}$ is a contraction, since the magnitude of its derivative is less than unity. □

We proceed with the main result for slow evolution from the continuation boundary, based on the previous Hölder continuity in (53).

THEOREM 3. *Let ε, M and $\mathcal{M}$ be given constants with $\varepsilon < M$ and $\mathcal{M}\varepsilon < M$. Let X be a Banach space with norm $\|\cdot\|$, and let $g \in X$. Let $\mathcal{C}$ be a linear or nonlinear continuation problem from the data g for the X-valued function $v(x,\cdot)$, $0 \leq x \leq l$, where $\|v(0,\cdot)\| \leq M$ and $\|v(l,\cdot) - g\| \leq \varepsilon$. Let $\mathcal{C}$ be such that the difference of any two possible continuations satisfies (50). If the solutions also satisfy $\|v(x_0,\cdot) - v(0,\cdot)\| \leq \mathcal{M}\varepsilon$ for some known $x_0 > 0$ with $x_0 > lx_0^*$, where x_0^* is defined in (54), then*

$$\|v_1(x,\cdot) - v_2(x,\cdot)\| \leq 2\Gamma^{1-\frac{x}{l}}\varepsilon \ , \tag{59}$$

where Γ is the constant defined in Lemma 5. Moreover, $\Gamma \ll \frac{M}{\varepsilon}$ if $x_0^* \ll \frac{x_0}{l}$.

Proof. On assumption, the difference of any two continuations, introduced in the proof of Theorem 2, and the solution satisfy

$$\begin{gathered} \|\Delta v(x,\cdot)\| \leq \Lambda^{1-\frac{x}{l}}\delta^{\frac{x}{l}} \ , \quad 0 \leq x \leq l \ , \\ \|v(x_0,\cdot) - v(0,\cdot)\| \leq \mathcal{M}\delta \ , \quad x_0 > 0 \ , \quad \tfrac{x_0}{l} > x_0^* \ , \end{gathered} \tag{60}$$

where $\Lambda = 2M$ and $\delta = 2\varepsilon$. The triangle inequality yields the estimate

$$\begin{gathered} \|\Delta v(x,\cdot)\| \leq \|\Delta v(0,\cdot)\|^{1-\frac{x}{l}} \|\Delta v(l,\cdot)\|^{\frac{x}{l}} \leq \\ \left(\|\Delta v(x_0,\cdot) - \Delta v(0,\cdot)\| + \|\Delta v(x_0,\cdot)\|\right)^{1-\frac{x}{l}} \|\Delta v(l,\cdot)\|^{\frac{x}{l}} \ , \end{gathered} \tag{61}$$

inserting (60) gives

$$\|\Delta v(x_0,\cdot)\| \leq \left(\mathcal{M}\delta + \Lambda^{1-\frac{x_0}{l}}\delta^{\frac{x_0}{l}}\right)^{1-\frac{x_0}{l}} \delta^{\frac{x_0}{l}} \ . \tag{62}$$

Here, the initial estimate $\|\Delta v(x_0,\cdot)\|_{(1)} \leq \Lambda^{1-\frac{x_0}{l}}\delta^{\frac{x_0}{l}}$ has been used in (61) to produce a new estimate, $\|\Delta v(x_0,\cdot)\|_{(2)}$, given by (62). We can now insert (62) back into (61) to produce a third estimate, and so on. At the nth step of that iteration, we get the estimate $\|\Delta v(x_0,\cdot)\|_{(n)} \leq Z_n^{1-\frac{x_0}{l}}\delta^{\frac{x_0}{l}}$, with

$$Z_1 = \Lambda \ , \quad \frac{Z_k}{\delta} = \mathcal{M} + \left(\frac{Z_{k-1}}{\delta}\right)^{1-\frac{x_0}{l}} \ , \quad k > 1 \ . \tag{63}$$

As $n \uparrow \infty$, $Z_n \to \Gamma\delta$, with Γ defined in Lemma 5. Hence, $\|\Delta v(x_0,\cdot)\| \leq \Gamma^{1-\frac{x_0}{l}}\delta$ and if we insert this into (61) keeping in mind the second inequality of (60) and the transcendental

equation (55) for Γ, we obtain the final result

$$\begin{gathered}\|\Delta v(x,\cdot)\| \leq \left(\|\Delta v(x_0,\cdot) - \Delta v(0,\cdot)\| + \|\Delta v(x_0,\cdot)\|\right)^{1-\frac{x}{l}} \|\Delta v(l,\cdot)\|^{\frac{x}{l}} \leq \\ \left(\mathcal{M}\delta + \Gamma^{1-\frac{x_0}{l}}\delta\right)^{1-\frac{x}{l}} \|\Delta v(l,\cdot)\|^{\frac{x}{l}} = (\Gamma\delta)^{1-\frac{x}{l}} \|\Delta v(l,\cdot)\|^{\frac{x}{l}} \leq \\ (\Gamma 2\varepsilon)^{1-\frac{x}{l}} (2\varepsilon)^{\frac{x}{l}} = 2\Gamma^{1-\frac{x}{l}}\varepsilon \ , \quad 0 \leq x \leq l\end{gathered} \tag{64}$$

The statement $\Gamma \ll \frac{M}{\varepsilon}$ if $x_0^* \ll \frac{x_0}{l}$ is readily shown using the last inequality of (56) in Lemma 5. □

REMARK 3. For $x_0 = lx_0^*$, the result of Theorem 3 degenerates from improved Hölder continuity to the ordinary Hölder continuity of Theorem 2. The farther from the continuation boundary we can apply the SECB-constraint, the slower the error propagation is, and the better the obtained stability result is.

EXAMPLE 2. Consider the SECB (Slow Evolution from the Continuation Boundary), with $\varepsilon = 10^{-2}M$, $l = 1$, $\mathcal{M} = 3M$, giving $x_0^* \approx 0.0066$. If we choose $x_0/l = 50x_0^* \approx 0.33$, the solution of (55) is $\Gamma \approx 6.50 \ll M/\varepsilon = 10^2$. This yields the improved Hölder continuity $\|v_1(0,\cdot) - v_2(0,\cdot)\| \leq 0.13M$, which depending on the application may be a significantly better bound than the noise contamination characteristic of the ordinary Hölder continuity.

4. Regularization

4.1. General. Regularization can be used as a unifying term for various strategies of constraining ill-posed inverse problems in order to make the solution well-posed, i.e., achieve existence, uniqueness and stability. Since the ill-posed nature of the original, unregularized inverse problem generally is due to loss of information that cannot be recovered in the course of solution, regularization essentially also involves use of additional information about the solution. Such additional information can be, e.g., *a priori* knowledge of input data error (41) and the solution bound (42). There are two alternative approaches to regularization, where one puts constraints on either the space of permissible input/output data or on the set of mathematical models describing the inverse problem. Above we gave a typical example of the former approach. Frequently, a combination of both approaches may be motivated.

The quarter plane and finite geometry problems are linear inverse problems, for which a well-established regularization theory exists. However, nonlinear inverse problems, of which the boundary identification problem is an example, yet lack a unified regularization theory. A solution method containing ideas common to both linear and nonlinear inverse problems is *Tikhonov regularization* [**21**], which can be formulated as an optimization problem. Thus, in transforming the problem, Tikhonov regularization is an example of a model-space constraining method. Using the notation in the introduction above, we can write down this problem as

$$\min_f \|A(f) - g_m\|^2 + \alpha \|f\|^2 \ . \tag{65}$$

There is a great variety of schemes how to choose the *regularization parameter* α. In the so-called *a priori* methods the choice is based solely on the properties of the operator A, while the *a posteriori* methods are based on the residual $A(f) - g_m$. In practice, visual evaluation of the solution serves as an additional *a posteriori* criterion. Hence, a characteristic common to all of the a posteriori methods is the dependence on additional information on input data

and/or solution properties. We will not go into these specific methods at this stage, since our regularization method does not fall into the category of Tikhonov methods according to (65).

In the linear case (i.e., when A is a linear operator) for the quarter plane problem, solution of (65) is equivalent to a filtering approach **[32, 34, 12]**. The idea of filtering is present in many regularization methods, such as mollification **[34]** and approximation by a well-posed equation **[19]** for linear problems. In the nonlinear inverse problem of boundary identification, we will attempt a bounded operator method which is basically a spectral cut-off filtering approach.

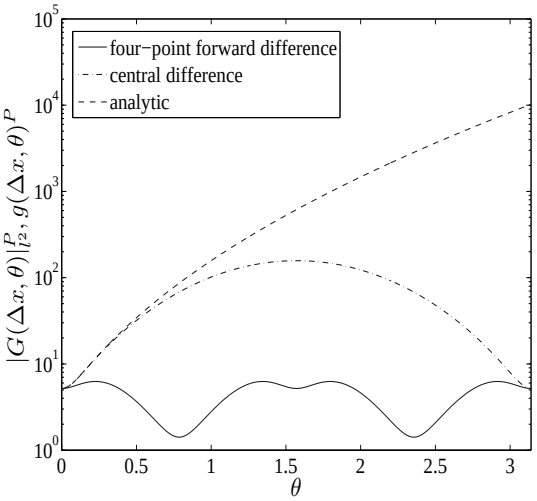

FIGURE 2.1. Amplification factors for the analytical case, two-point central (S3 in **[13]**) and four-point forward difference approximations (68).

4.2. Discretization. In a numerical solution for a finite time interval of the quarter plane or finite geometry problem, some type of discretization is needed to approximate the differential or integral operators in the problem formulation. Thus, this is a model-space constraining method. Hence, finite differences might be used in the former and quadratures in the latter case. Several workers have observed that discretization as such has a regularizing effect, both for finite difference schemes, quadratures and collocation methods **[12, 13, 14, 19, 30]**. Originally, only filtering of input data was used to remove high frequency components and some simple discretization adopted to solve the sideways heat equation just like any well-posed initial value problem. Good final results were reported in these calculations, **[35, 24, 36]** although it was later noted that the problem was still ill-posed and rounding errors were necessarily magnified severely in the course of computation. The explanation for the success despite this ill-posedness was the regularizing effect of the discretization schemes used.

Applying the Lax-Richtmyer theory **[42]** the discretized solution operator of the finite geometry problem, viewed as the mapping from the noisy sensor data to the unknown boundary,

can be investigated **[13]**. The finite geometry problem (21, 22) can be discretized in both space and time to, e.g., an explicit Euler space marching scheme

$$\begin{aligned}\begin{bmatrix} u \\ u_x \end{bmatrix}(l-(x+\Delta x)) &= \left(\Delta x \begin{bmatrix} 0 & I \\ \frac{\partial}{\partial t} & 0 \end{bmatrix} + I\right)\begin{bmatrix} u \\ u_x \end{bmatrix}(l-x) \\ &:= C(\Delta x, \Delta t)\begin{bmatrix} u \\ u_x \end{bmatrix}(l-x)\ .\end{aligned} \tag{66}$$

Introducing the Fourier image $G(\Delta x, \theta)$, in terms of the normalized frequency θ, of $C(\Delta x, \Delta t)$, one has the relation

$$\|C^P\| = \max_{0\le\theta\le\pi} |G(\theta)^P|_{l^2}, \tag{67}$$

where $\|\cdot\|$ denotes the L^2 norm in the time variable, $|\cdot|_{l^2}$ the Euclidean norm and P is the maximum number of spatial steps required to reach the desired boundary. The matrix $G(\theta)$ is 2×2 and, e.g., a four-step forward difference approximation to $\frac{\partial}{\partial t}$ yields

$$G(\theta) = \begin{bmatrix} 1 & \Delta x \\ \frac{\Delta x}{4\Delta t}\left(\mathrm{e}^{4i\theta}-1\right) & 0 \end{bmatrix}. \tag{68}$$

For comparison, the corresponding analytical solution operator for one space step Δx is a convolution kernel with the Fourier image $\mathrm{e}^{\Delta x\sqrt{i\theta/\Delta t}}$. The magnitude of this is $g(\Delta x,\theta) = \mathrm{e}^{\Delta x\sqrt{|\theta|/2\Delta t}}$ to which $|G(\Delta x,\theta)|_{l^2}$ is a discrete approximation. Thus, marching the input data P spatial steps to reach the desired boundary, amplifies the noise by a factor $g(\Delta x,\theta)^P$. Alternative discretizations are treated extensively by Carasso **[13]**, including the cases with central difference and the forward difference approximation of $\frac{\partial}{\partial t}$. For the sake of illustration, an example computation with exaggerated parameter values was performed, results of which are depicted in Fig. 2.1 together with the analytic amplification factor $g(\Delta x,\theta)^P$ for the parameter values $\Delta t = 0.5$, $\Delta x = 5\cdot 10^{-4}$ and $P = 10^4$. From Fig. 2.1 it appears that the regularization in (68) performs well with respect to error growth.

Eldén **[19]** gave an error estimate for the central difference approximation of $\frac{\partial}{\partial t}$ amounting (for $\frac{M}{\varepsilon} > \mathrm{e}^{-5}$) to a result similar to (46) but with the factor 3 instead of 2 on the r.h.s. Other cases for $\frac{M}{\varepsilon}$ are also treated, yielding more complicated error estimates. This suboptimal stability can be achieved with the discretization $\Delta t = \frac{1}{2\left(\log\frac{M}{\varepsilon}\right)^2}$. Thus, the larger the noise-to-signal ratio the longer the time step should be in order to stabilize the computation. One would also expect this to affect the spatial discretization. It turns out that an explicit method, like e.g. (66) or at most a fourth-order Runge-Kutta method, is sufficient for longer time steps in the case $\frac{M}{\varepsilon} > \mathrm{e}^{-5}$, whereas for shorter time steps an implicit space marching method might be necessary **[20]**. The mesh size of the spatial discretization is in all cases determined by the requirement that the eigenvalues of the discretized system matrix in the space marching scheme stay inside the particular stability region of the ex/implicit scheme.

4.3. Mollification. Mollification is a typical data constraining method, which maps the measurement data into classes where the problem is well-posed through "smoothing" the improper data. In many cases this restriction of data constitutes the mollification but one should

also think about ways of solving the problem in a stable way. In addition to a brief but detailed review on mollification, Hào **[25]** considered this aspect by obtaining error estimates that were minimized with respect to a mollification parameter.

Let A^{-1} be a linear and unbounded operator on the Banach space X with the norm $\|\cdot\|$. We would like to calculate $f := A^{-1}g$, when g is given approximately by g_m (not necessarily in the domain of A^{-1}) according to (41). Hào **[25]** proposes the following mollification method for solving the problem:

(1) Establish a sequence of subspaces X_ν, $\nu > 0$, of X such that $X_\nu \supset X_\varsigma$ if $\nu > \varsigma$, $X_\infty \equiv X$, and in which the problem is well-posed: Then, there exists a function $a(\cdot,\cdot)$ such that

$$\|A^{-1}g\| \leq a(\nu, \|g\|) \ , \quad \text{if } g \in X_\nu \cap D(A^{-1}) \ .$$

(2) Find a sequence of operators $\mathsf{M}_\nu : X \mapsto X_\nu$ with the properties:
   (a) there exists a function $\mathsf{m}(\cdot,\cdot)$ such that $\|\mathsf{M}_\nu g - g\| \leq \mathsf{m}(\nu, \|g\|)$ with $\lim_{\nu\to\infty} \mathsf{m}(\nu, \|g\|) = 0$ when g is fixed. (Approximation property),
   (b) $\mathsf{M}_\nu A^{-1} \equiv A^{-1}\mathsf{M}_\nu$,
   (c) $\|\mathsf{M}_\nu\| \leq \mathsf{c}$, where c is a positive constant (in case M_ν is the orthogonal projection of X onto X_ν we have $\|\mathsf{M}_\nu\| = 1$).

(3) If g is given approximately by g_m according to (41) we can mollify it according to $g_m \mapsto \mathsf{M}_\nu g_m \in X_\nu \cap D(A^{-1})$. Thus, instead of doing the ill-posed calculation $f = A^{-1}g_m$ we calculate $f_\nu = A^{-1}\mathsf{M}_\nu g_m$.

The idea is to solve the problem stably in X_ν, keeping in mind that the original data g_m are "transferred" to $X_\nu \cap D(A^{-1})$ in the process. Property (2a) describes how well the space X_ν approximates the space X. Property (2b) is somewhat restrictive, although it is frequently valid. This is the case when M_ν is a convolution operator and A^{-1} is a pseudodifferential operator with constant coefficients, e.g., in solving the sideways heat conduction equation **[34]**. With these properties, Hào **[25]** obtained the error estimate

$$\|f - f_\nu\| \leq \mathsf{m}(\nu, \|A^{-1}g\|) + a(\nu, \|\mathsf{M}_\nu(g - g_m)\|) \ . \tag{69}$$

The total error is hence made up of a contribution from propagating measurement error and a contribution from the approximation error introduced through the smoothing action of the mollification. The optimal value for the mollification parameter ν minimizes the r.h.s. in (69). From a computational point of view, mollifying noisy data is economical only in more severe situations. For moderately noisy measurement data, direct discretization is more practical.

4.4. Approximation by a well-posed equation. The idea of approximating an ill-posed problem by a well-posed one can be regarded as a model-constraining approach. For instance, the idea of turning the (x,t)-coordinate system slightly, say to $(x - \epsilon t, t + \epsilon x)$ for a small number ϵ, leads to a well-posed hyperbolic partial differential equation containing a mixed derivative. The transition to a well-posed hyperbolic PDE, i.e., the telegraph equation (70), has also been suggested on physical grounds, e.g., in **[33]**. Inspired by this, Weber **[49]** studied a hyperbolic approximation to the finite geometry problem on $t \in [0,T]$, i.e., computing the temperature $f(t) = v(0,t)$ at the remote end of a finite geometry in

$$\tilde{v}_{xx}(x,t) = \gamma^2 \tilde{v}_{tt}(x,t) + \tilde{v}_t(x,t) \ , \tag{70}$$

$$
\begin{array}{c}
\tilde{v}(l,t) = g(t) \ , \\
\tilde{v}_x(l,t) = h(t) \ , \\
\tilde{v}(x,0) = \tilde{v}_0 \ , \\
\tilde{v}(x,T) = \tilde{v}_T \ , \\
x \in [0,l], \quad t \in [0,T] \ .
\end{array} \tag{71}
$$

This can be studied as an initial-boundary value problem if the specified functions for the temperature and flux at l are considered initial values and the functions $\tilde{v}(x,0)$, $\tilde{v}(x,T)$ as boundary values. From the solution to this initial-boundary value problem [**48**], a Volterra integral equation of the second kind can be derived for the unknown surface temperature $f(t) = v(0,t)$. Since such an equation is well-posed, the approach leads to a stable algorithm as shown in a number of example computations using an explicit finite difference scheme for (70,71) with $\gamma = 0.01$. The computed surface temperature was compared with known analytic solutions, but no analysis of the approximation error was provided.

Similar ideas were applied to the quarter plane problem (16,17). Eldén initially tried adding a higher order derivative ($\gamma^2 \tilde{v}_{xxtt}$) [**17**]. However, this led to a need for a requirement that the solution be bounded for long times, - a requirement that is not present in the original quarter plane problem. This difficulty turned attention to the mixed-derivative formulation, mentioned above, obtainable by turning the coordinate system [**18**]. In an example error estimate, a choice of $\gamma = \left(2 \log \frac{M}{\varepsilon}\right)^{-1}$ yielded an error somewhat inferior to $3M^{1-x/l}\varepsilon^{x/l}$ for the difference between the noiseless solution to the quarter plane problem and the one obtained by using the approximation (70) with noisy measurements. This should be compared to the optimal, intrinsic error in the problem, expressed by Theorem 2.

Murio and Roth [**37**] combined the approximation (70) applied to the quarter plane problem with a mollification in $L_2(-\infty, \infty)$. The mollification parameter was in this case determined from the requirement that the difference in norms between the noisy measurement and its mollification be equal to the error ε. In the computations, the second order Volterra integral equation was discretized and solved together with a discrete convolution for the mollification. Considering the fact that discretization in the computation adds up to the error introduced by the approximation, we are inclined to argue that although theoretically appealing, direct discretization appears a better choice for regularization. For more severe measurement errors, one might opt for mollifying the data prior to computation.

5. Solving the sideways heat equation as a Cauchy-problem

As indicated with the discretization scheme (66), the sideways heat equation can be considered a Cauchy-problem in the spatial variable, i.e., we can use the block-operator form

$$
\begin{bmatrix} v(t) \\ v_x(t) \end{bmatrix}_x (l-x) \quad = \quad \begin{bmatrix} 0 & I \\ \frac{\partial}{\partial t} & 0 \end{bmatrix} \begin{bmatrix} v(t) \\ v_x(t) \end{bmatrix} (l-x) \tag{72}
$$

with the "initial" condition

$$
\begin{array}{c}
\begin{bmatrix} v \\ v_x \end{bmatrix} (0) = \begin{bmatrix} g(t) \\ h(t) \end{bmatrix} \ , \\
v(x,0) = 0 \ , \\
x \in [0,l], \quad t \in [0,\infty) \ .
\end{array} \tag{73}
$$

In this formulation, the finite geometry problem (21, 22) is treated as an "initial value problem" in the variable x. However, a significant complication arises when we apply this idea in practice.

5.1. A fundamental difficulty. The fundamental difficulty with the Cauchy-problem formulation above is time differentiation in the block-operator of (72), making the operator unbounded [**29**]. To overcome this, we need to regularize the formulation by finding a bounded approximation to the time differentiation. When applying a space marching scheme in the actual solution of the Cauchy problem, the quality of such an approximation is crucial in order to avoid excessive approximation error in the final solution. Our approach to this, which will be described below, consists of working in the Hilbert space $L_2(0,\infty)$ with a uniform approximation to $\frac{\partial}{\partial t}$ in the frequency plane up to some cutoff frequency.

5.2. Ideas for application to boundary identification. The Cauchy-problem formulation also provides an opening for boundary identification, i.e., computing the function $s(t)$ in

$$v_{xx}(x,t) = v_t(x,t) \ , \tag{74}$$

$$\begin{gathered} v(0,t) = g(t) \ , \quad v_x(0,t) = h(t) \ , \\ v(s(t),t) = f(t) \ , \quad v(x,0) = 0 \ , \\ x \in [0, s(t)], \quad t \in [0,\infty) \ , \end{gathered} \tag{75}$$

from measured $g(t)$, $h(t)$. Writing (74, 75) as a Cauchy-problem and space marching from the known functions $g(t)$, $h(t)$ at $x = 0$ until the known state $f(t)$ is reached presents itself as a strategy for finding $s(t)$ if the "marching distance" for each time is recorded.

CHAPTER 3

Boundary Identification

Before proceeding with the space marching approach to solving (74, 75), we demonstrate and discuss two classical solution methods, described and derived in the paper **[50]**. The first is based on a weak solution together with a linearization approach while the second is based on the fundamental solution of the finite plane problem. In both cases, we obtain an integral equation for the desired boundary movement $s(t)$. Subsequently, we develop the strategy suggested above for boundary identification through reformulation as a Cauchy-problem and space marching. Finally, we describe how this approach works for a few numerical examples. These were implemented using the software package MATLAB®. The partial differential equations for the direct problems were solved through built-in functions using the method of lines, i.e., by converting them to systems of ordinary differential equations in the time variable. Numerical integration was carried out using built-in quadrature subroutines.

1. A simple case - analytical solution through linearization

Since the domain in (74, 75) of $v(x,t)$ is time-dependent due to the boundary movement, our first task is to obtain a fixed domain by the transformation $\eta = \frac{x}{s(t)}$, $s(t) \in C^1([0,\infty))$ for $\vartheta(\eta,t)$, cf. Counterexample 1. Then, $\vartheta(\eta,t)$ satisfies

$$\frac{1}{s^2(t)}\vartheta_{\eta\eta}(\eta,t) + \frac{\eta s'(t)}{s(t)}\vartheta_\eta(\eta,t) = \vartheta_t(\eta,t)\ , \tag{76}$$

$$\begin{gathered}\vartheta(0,t) = g(t)\ ,\quad \tfrac{1}{s(t)}\vartheta_\eta(0,t) = h(t)\ ,\\ \vartheta(1,t) = f(t)\ ,\quad \vartheta(\eta,0) = 0\ ,\\ \eta \in [0,1],\quad t \in [0,\infty)\ ,\end{gathered} \tag{77}$$

for known piecewise continuous $f(t)$ and measured piecewise continuous $g(t)$, $h(t)$. Now, we suppose that the problem is normalized so that $s(t) = 1 + d(t)$, where $d(t)$ is a small (perturbation) function measured in an appropriate norm. Similarly, consider the solution $\vartheta(\eta,t) = V(\eta,t) + r(\eta,t)$ to (76, 77) as a sum of the solution, $V(\eta,t)$, for $d(t) = 0$ and the expectedly small, norm-bounded perturbation, $r(\eta,t)$, caused by the small, norm-bounded function $d(t)$. It should be noted that we do not propose to show that if d is small then so is r. This is a topic for future work. With the above definitions, $V(\eta,t)$ can be chosen to satisfy the initial-boundary value problem

$$V_{\eta\eta}(\eta,t) = V_t(\eta,t)\ , \tag{78}$$

$$\begin{gathered} V_\eta(0,t) = h(t) \ , \\ V(1,t) = f(t) \ , \quad V(\eta,0) = 0 \ , \\ \eta \in [0,1], \quad t \in [0,\infty) \ . \end{gathered} \tag{79}$$

Considering the solution $\vartheta(\eta,t) = V(\eta,t) + r(\eta,t)$ in (76, 77) leads to

$$\begin{gathered} \tfrac{1}{(1+d(t))^2}\left(V_{\eta\eta}(\eta,t) + r_{\eta\eta}(\eta,t)\right) + \tfrac{\eta d'(t)}{1+d(t)}\left(V_\eta(\eta,t) + r_\eta(\eta,t)\right) = \\ V_t(\eta,t) + r_t(\eta,t) \ , \end{gathered} \tag{80}$$

$$\begin{gathered} V(0,t) + r(0,t) = g(t) \ , \quad V_\eta(0,t) + r_\eta(0,t) = (1+d(t))\, h(t) \ , \\ V(1,t) + r(1,t) = f(t) \ , \quad V(\eta,0) + r(\eta,0) = 0 \ , \\ \eta \in [0,1], \quad t \in [0,\infty) \ . \end{gathered} \tag{81}$$

Combination of the boundary conditions (79) with (81) yields the conditions for the perturbation to the solution, $r(\eta,t)$,

$$\begin{gathered} r(0,t) = g(t) - V(0,t) \ , \quad r_\eta(0,t) = d(t)h(t) \ , \\ r(1,t) = 0 \ , \quad r(\eta,0) = 0 \ , \\ \eta \in [0,1], \quad t \in [0,\infty) \ . \end{gathered} \tag{82}$$

Our task is now to compute an approximation of the perturbation $d(t)$ with the help of (80), which in the most general setting can be considered a nonlinear ordinary differential equation for $d(t)$. By noting (78), (80) can be cast in the form

$$\begin{gathered} d'(t)(1+d(t))\eta\left(V_\eta(\eta,t) + r_\eta(\eta,t)\right) = \\ d(t)(2+d(t))\left(V_t(\eta,t) + r_t(\eta,t)\right) + r_t(\eta,t) - r_{\eta\eta}(\eta,t) \ . \end{gathered} \tag{83}$$

We proceed by dropping all second order and higher terms, i.e., those containing products of small, norm-bounded quantities like $d^2(t)$, $d'(t)d(t)$, $d'(t)r_\eta(\eta,t)$ and $d(t)r_t(\eta,t)$ in (83), assuming that the first-order partial derivatives of the small, norm-bounded perturbation $r(\eta,t)$ are small. Hence, we obtain the equation

$$r_t(\eta,t) - r_{\eta\eta}(\eta,t) \approx \eta d'(t) V_\eta(\eta,t) - 2d(t)V_t(\eta,t) \ , \tag{84}$$

Our objective is to compute an estimate of $d(t)$ using (84). Since the perturbation $r(\eta,t)$ to the solution depends on $d(t)$ and the spatial position η, we introduce the following auxiliary result:

LEMMA 6. *Let $\psi(\eta,t)$ satisfy the* backward heat equation $\psi_t(\eta,t) + \psi_{\eta\eta}(\eta,t) = 0$ *for $\eta \in (0,1)$ and $t \in (0,\infty)$, with $\psi(1,t) = 0$. Then, for $\tau \in (0,\infty)$, we have*

$$\begin{gathered} \int_0^\tau \int_0^1 \psi(\eta,t)\left(r_t(\eta,t) - r_{\eta\eta}(\eta,t)\right) \mathrm{d}\eta \mathrm{d}t = \\ \int_0^1 \psi(\eta,\tau) r(\eta,\tau) \mathrm{d}\eta + \int_0^\tau \psi(0,t) r_\eta(0,t) - \psi_\eta(0,t) r(0,t) \mathrm{d}t \ . \end{gathered} \tag{85}$$

Proof. We start by splitting up the integral and apply Fubini's Theorem to change the order of integration and integrate the first term by parts according to

$$\begin{gathered} \int_0^\tau \int_0^1 \psi(\eta,t) r_t(\eta,t) \mathrm{d}\eta \mathrm{d}t = \\ \int_0^1 \Big/_0^\tau \psi(\eta,t) r(\eta,t) \mathrm{d}\eta - \int_0^1 \int_0^\tau \psi_t(\eta,t) r(\eta,t) \mathrm{d}t \mathrm{d}\eta = \\ \int_0^1 \psi(\eta,\tau) r(\eta,\tau) \mathrm{d}\eta + \int_0^1 \int_0^\tau \psi_{\eta\eta}(\eta,t) r(\eta,t) \mathrm{d}t \mathrm{d}\eta \ . \end{gathered} \tag{86}$$

Here, the initial value for $r(\eta,t)$ in (82) was used as well as the assumption that $\psi(\eta,t)$ satisfies the backward heat equation. We proceed with the second integral on the left hand side of (85), using Fubini's Theorem once again to integrate by parts repeatedly in η:

$$\begin{aligned}
&\int_0^1\int_0^\tau \psi(\eta,t)r_{\eta\eta}(\eta,t)\mathrm{d}t\mathrm{d}\eta = \\
&\int_0^\tau \Big/_0^1 \psi(\eta,t)r_\eta(\eta,t)\mathrm{d}t - \int_0^\tau\int_0^1 \psi_\eta(\eta,t)r_\eta(\eta,t)\mathrm{d}\eta\mathrm{d}t = \\
&-\int_0^\tau \psi(0,t)r_\eta(0,t)\mathrm{d}t - \int_0^\tau\int_0^1 \psi_\eta(\eta,t)r_\eta(\eta,t)\mathrm{d}\eta\mathrm{d}t = \\
&-\int_0^\tau \left(\psi(0,t)r_\eta(0,t) + \Big/_0^1 \psi_\eta(\eta,t)r(\eta,t)\right)\mathrm{d}t + \int_0^\tau\int_0^1 \psi_{\eta\eta}(\eta,t)r(\eta,t)\mathrm{d}\eta\mathrm{d}t = \\
&-\int_0^\tau \left(\psi(0,t)r_\eta(0,t) - \psi_\eta(0,t)r(0,t)\right)\mathrm{d}t + \int_0^\tau\int_0^1 \psi_{\eta\eta}(\eta,t)r(\eta,t)\mathrm{d}\eta\mathrm{d}t\ .
\end{aligned} \tag{87}$$

Using (86) and (87) as well as the assumption $\psi_t(\eta,t)+\psi_{\eta\eta}(\eta,t)=0$, we obtain the desired result

$$\begin{aligned}
&\int_0^\tau\int_0^1 \psi(\eta,t)\left(r_t(\eta,t)-r_{\eta\eta}(\eta,t)\right)\mathrm{d}\eta\mathrm{d}t = \\
&\int_0^1 \psi(\eta,\tau)r(\eta,\tau)\mathrm{d}\eta + \int_0^1\int_0^\tau \psi_{\eta\eta}(\eta,t)r(\eta,t)\mathrm{d}t\mathrm{d}\eta + \\
&\int_0^\tau \left(\psi(0,t)r_\eta(0,t)-\psi_\eta(0,t)r(0,t)\right)\mathrm{d}t - \int_0^\tau\int_0^1 \psi_{\eta\eta}(\eta,t)r(\eta,t)\mathrm{d}\eta\mathrm{d}t\ .\ \square
\end{aligned} \tag{88}$$

This result allows us to get rid of the spatial variable η in (84), by considering averages weighted spatially by the function $\psi(\eta,t)$. Our choice for $\psi(\eta,t)$ is arbitrary, as long as the backwards heat equation and a zero boundary condition at $\eta=1$ are satisfied. The boundary conditions (82) can be used for $r_\eta(0,t)$ and $r(0,t)$. Consequently, everything except the integral $I_r(\tau)=\int_0^1\psi(\eta,\tau)r(\eta,\tau)\mathrm{d}\eta$ is computable in our averaged version of (84)

$$\begin{aligned}
&\int_0^\tau\int_0^1 \psi(\eta,t)\left(r_t(\eta,t)-r_{\eta\eta}(\eta,t)\right)\mathrm{d}\eta\mathrm{d}t = \\
&\int_0^1 \psi(\eta,\tau)r(\eta,\tau)\mathrm{d}\eta + \int_0^\tau \psi(0,t)r_\eta(0,t) - \psi_\eta(0,t)r(0,t)\mathrm{d}t \approx \\
&\int_0^\tau\int_0^1 \eta d'(t)\psi(\eta,t)V_\eta(\eta,t) - 2d(t)\psi(\eta,t)V_t(\eta,t)\mathrm{d}\eta\mathrm{d}t\ .
\end{aligned} \tag{89}$$

Differentiating (89) with respect to τ leads to the approximate relation

$$\begin{aligned}
&I_r'(\tau) + \psi(0,\tau)r_\eta(0,\tau) - \psi_\eta(0,\tau)r(0,\tau) \approx \\
&d'(\tau)\int_0^1 \eta\psi(\eta,\tau)V_\eta(\eta,\tau)\mathrm{d}\eta - 2d(\tau)\int_0^1 \psi(\eta,\tau)V_{\eta\eta}(\eta,\tau)\mathrm{d}\eta\ .
\end{aligned} \tag{90}$$

However, the perturbation $r(\eta,\tau)$ to the solution is norm-bounded. Furthermore, if $\tau>0$ and either $d(t)$ or $h(t)$ or both decay to zero, the support of the flux $r_\eta(0,t)$ in (82) will be localized to small times and the contribution to (89) from the integral $I_r'(\tau)$ can be disregarded. Consider the auxiliary

LEMMA 7. *Let $\psi(\eta,\tau)$ satisfy the* backward heat equation *and $r(\eta,\tau)$ the boundary conditions (77, 79). Then, with $\|\cdot\|$ denoting the supremum norm, we have the estimate*

$$\begin{aligned}
&\|I_r'(\tau)\| \le \left\|1-\tfrac{1}{s^2(\tau)}\right\| \|I_{\vartheta,1}(\tau) + \psi_\eta(1,\tau)f(\tau) - \psi_\eta(0,\tau)g(\tau)\| + \\
&\tfrac{\|d'(\tau)\|}{\|s(\tau)\|}\|I_{\vartheta,2}(\tau)\| + \|\psi_\eta(0,\tau)\|\,\|g(\tau)-V(0,\tau)\| + \tfrac{\|d(\tau)\|}{\|s(\tau)\|}\|\psi(0,\tau)\|\,\|h(\tau)\|\ ,
\end{aligned} \tag{91}$$

where

$$
\begin{array}{l}
I_{\vartheta,1}(\tau) = \int_0^1 \psi_\tau(\eta,\tau)\vartheta(\eta,\tau)\ \mathrm{d}\eta\ , \\
I_{\vartheta,2}(\tau) = \int_0^1 \left(\psi(\eta,\tau) + \eta\psi_\eta(\eta,\tau)\right)\vartheta(\eta,\tau)\ \mathrm{d}\eta\ .
\end{array} \tag{92}
$$

Proof. Here, we are allowed to differentiate under the integral sign, since $\psi_\tau(\eta,\tau)$ is continuous and $r_\tau(\eta,\tau)$ exists for $0 < \eta < 1$, $\tau > 0$. Hence, integrating by parts twice, we can rather tediously compute

$$
\begin{array}{c}
I_r'(\tau) = \int_0^1 \psi_\tau(\eta,\tau)r(\eta,\tau)\mathrm{d}\eta + \int_0^1 \psi(\eta,\tau)r_\tau(\eta,\tau)\mathrm{d}\eta = \\
\int_0^1 \psi_\tau(\eta,\tau)r(\eta,\tau)\mathrm{d}\eta + \int_0^1 \psi(\eta,\tau)\left(\vartheta_\tau(\eta,\tau) - V_\tau(\eta,\tau)\right)\mathrm{d}\eta = \\
\int_0^1 \psi_\tau(\eta,\tau)r(\eta,\tau)\mathrm{d}\eta + \frac{1}{s^2(\tau)}\int_0^1 \psi(\eta,\tau)\vartheta_{\eta\eta}(\eta,\tau)\mathrm{d}\eta + \\
\frac{s'(\tau)}{s(\tau)}\int_0^1 \eta\psi(\eta,\tau)\vartheta_\eta(\eta,\tau)\mathrm{d}\eta - \int_0^1 \psi(\eta,\tau)V_{\eta\eta}(\eta,\tau)\mathrm{d}\eta =
\end{array} \tag{93}
$$

$$
\begin{array}{c}
\int_0^1 \psi_\tau(\eta,\tau)r(\eta,\tau)\mathrm{d}\eta + \\
\frac{1}{s^2(\tau)}\left(\Big/_0^1 \psi(\eta,\tau)\vartheta_\eta(\eta,\tau) - \int_0^1 \psi_\eta(\eta,\tau)\vartheta_\eta(\eta,\tau)\mathrm{d}\eta\right) + \\
\frac{s'(\tau)}{s(\tau)}\left(\Big/_0^1 \eta\psi(\eta,\tau)\vartheta(\eta,\tau) - \int_0^1 \left(\psi(\eta,\tau) + \eta\psi_\eta(\eta,\tau)\right)\vartheta(\eta,\tau)\mathrm{d}\eta\right) - \\
\Big/_0^1 \psi(\eta,\tau)V_\eta(\eta,\tau) + \int_0^1 \psi_\eta(\eta,\tau)V_\eta(\eta,\tau)\mathrm{d}\eta =
\end{array} \tag{94}
$$

$$
\begin{array}{c}
\int_0^1 \psi_\tau(\eta,\tau)r(\eta,\tau)\mathrm{d}\eta + \psi(0,\tau)h(\tau)\left(1 - \frac{1}{s(\tau)}\right) + \\
\frac{1}{s^2(\tau)}\left(\int_0^1 \psi_{\eta\eta}(\eta,\tau)\vartheta(\eta,\tau)\mathrm{d}\eta - \Big/_0^1 \psi_\eta(\eta,\tau)\vartheta(\eta,\tau)\right) - \\
\frac{s'(\tau)}{s(\tau)}\int_0^1 \left(\psi(\eta,\tau) + \eta\psi_\eta(\eta,\tau)\right)\vartheta(\eta,\tau)\mathrm{d}\eta + \\
\Big/_0^1 \psi_\eta(\eta,\tau)V(\eta,\tau) - \int_0^1 \psi_{\eta\eta}(\eta,\tau)V(\eta,\tau)\mathrm{d}\eta =
\end{array} \tag{95}
$$

$$
\begin{array}{c}
\int_0^1 \left(\psi_\tau(\eta,\tau)r(\eta,\tau) - \psi_{\eta\eta}(\eta,\tau)V(\eta,\tau) + \psi_{\eta\eta}(\eta,\tau)\frac{\vartheta(\eta,\tau)}{s^2(\tau)}\right)\mathrm{d}\eta + \\
\Big/_0^1 \psi_\eta(\eta,\tau)\left(V(\eta,\tau) - \frac{\vartheta(\eta,\tau)}{s^2(\tau)}\right) + \psi(0,\tau)h(\tau)\left(1 - \frac{1}{s(\tau)}\right) - \\
\frac{s'(\tau)}{s(\tau)}\int_0^1 \left(\psi(\eta,\tau) + \eta\psi_\eta(\eta,\tau)\right)\vartheta(\eta,\tau)\mathrm{d}\eta =
\end{array} \tag{96}
$$

$$
\begin{gathered}
\left(1-\tfrac{1}{s^2(\tau)}\right) I_{\vartheta,1}(\tau) - \tfrac{d'(\tau)}{s(\tau)} I_{\vartheta,2}(\tau) + \tfrac{d(\tau)}{s(\tau)}\psi(0,\tau)h(\tau) + \\
\left(1-\tfrac{1}{s^2(\tau)}\right) \int_0^1 \psi_\eta(\eta,\tau)\vartheta(\eta,\tau) + \int_0^1 \psi_\eta(\eta,\tau)\left(V(\eta,\tau)-\vartheta(\eta,\tau)\right) = \\
\left(1-\tfrac{1}{s^2(\tau)}\right)\left(I_{\vartheta,1}(\tau) + \psi_\eta(1,\tau)f(\tau) - \psi_\eta(0,\tau)g(\tau)\right) - \\
\tfrac{d'(\tau)}{s(\tau)} I_{\vartheta,2}(\tau) - \psi_\eta(0,\tau)\left(V(0,\tau)-g(\tau)\right) + \tfrac{d(\tau)}{s(\tau)}\psi(0,\tau)h(\tau) \ .
\end{gathered} \tag{97}
$$

Application of the triangle inequality for norms yields the desired estimate. □

REMARK 4. $\|I_r'(\tau)\|$ can be expected to be small when the perturbation $d(\tau)$ as well as its rate of change $d'(\tau)$ are moderate, i.e., the boundary function $s(\tau)$ is close to unity. Then, inspection of the right-hand side of (91) indicates that all terms are bounded and multiplied by a norm-moderated factor, since $g(\tau)$ approaches $V(0,\tau)$ for a small perturbation $d(\tau)$. Furthermore, $I_{\vartheta,1}(\tau)$ can be made as small as desired by an appropriate choice of the function $\psi(\eta,\tau)$. This choice also has some bearing on $I_{\vartheta,2}(\tau)$ as well as on the other norm factors of (91), which will be demonstrated in an example below.

Inserting boundary conditions from (82) into (90) and grouping terms, yields an approximate ordinary differential equation for $d(t)$

$$
a_1(\tau)d'(\tau) + a_0(\tau)d(\tau) \approx b(\tau) \ ,
$$

$$
\begin{gathered}
a_1(\tau) = \textstyle\int_0^1 \eta\psi(\eta,\tau)V_\eta(\eta,\tau)\mathrm{d}\eta \ , \\
a_0(\tau) = -h(\tau)\psi(0,\tau) - 2\textstyle\int_0^1 \psi(\eta,\tau)V_{\eta\eta}(\eta,\tau)\mathrm{d}\eta \ , \\
b(\tau) = -\psi_\eta(0,\tau)\left(g(\tau)-V(0,\tau)\right) \ .
\end{gathered} \tag{98}
$$

Unfortunately, situations are likely to arise, where this approximate differential equation is not stably solvable in the forward time direction, due to exponential growth caused by the opposite signs of $a_0(\tau)$ and $a_1(\tau)$, as will be seen in the following example. Nevertheless, the term $-h(\tau)\psi(0,\tau)$ in the coefficient $a_0(\tau)$ frequently dominates over the integrals, making it possible to approximate (98) with the algebraic relation $d(\tau) \approx \frac{b(\tau)}{a_0(\tau)}$. In our example, we were able to verify this by solving the approximate ODE backwards in time, indicating that the derivative term could be disregarded here.

EXAMPLE 3. We carry out a simulation for errorless data $f(\tau)$, $g(\tau)$, $h(\tau)$ in (77) and a theoretical boundary movement described by $d(\tau) = 0.2\sin\left(\frac{2\tau}{3}\right)$. Suppose that the function $h(\tau)$ is specified. Then, $g(\tau)$ can be computed by solving the direct problem (76, 77) for known functions $s(\tau) = 1 + d(\tau)$, i.e. the theoretical boundary movement, and $f(\tau)$. Subsequently, the inverse problem of estimating $d(\tau)$ can be solved according to our scheme above and the result compared with the theoretical boundary movement. This, we will outline below for various situations with different input data, however, first we need a function $\psi(\eta,\tau)$ [**50**].

DEFINITION 4. Consider, for the parameter $\alpha \in \mathbb{R}$, the function $\psi(\eta,\tau) := \phi_\alpha(\eta,\tau)$ in

$$
\begin{gathered}
2\sqrt{2\alpha}\ \psi(\eta,\tau) = 2\sqrt{2\alpha}\ \phi_\alpha(\eta,\tau) = \\
-\mathrm{e}^{-\sqrt{\frac{\alpha}{2}}(\eta-1)}\cos\left(\alpha\tau + \sqrt{\tfrac{\alpha}{2}}(\eta-1)\right) + \mathrm{e}^{\sqrt{\frac{\alpha}{2}}(\eta-1)}\cos\left(\alpha\tau - \sqrt{\tfrac{\alpha}{2}}(\eta-1)\right) + \\
\mathrm{e}^{-\sqrt{\frac{\alpha}{2}}(\eta-1)}\sin\left(\alpha\tau + \sqrt{\tfrac{\alpha}{2}}(\eta-1)\right) - \mathrm{e}^{\sqrt{\frac{\alpha}{2}}(\eta-1)}\sin\left(\alpha\tau - \sqrt{\tfrac{\alpha}{2}}(\eta-1)\right) \ .
\end{gathered} \tag{99}
$$

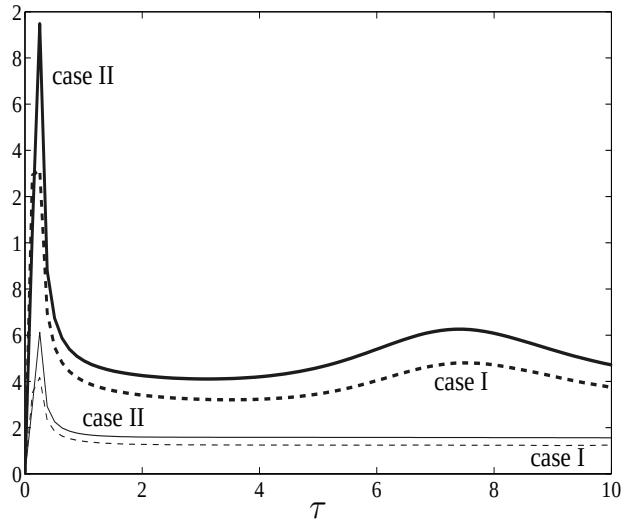

FIGURE 3.1. The bound (102) (thick markers) and the computed ratio $\left|\frac{a_1(\tau)}{a_0(\tau)}\right|$ (thin markers) for cases I (dashed line) and II (solid line).

Here, it can easily be checked that the conditions of Lemma 6 are fulfilled for (99), i.e. that $\psi(\eta,\tau)$ satisfies the backward heat equation with the boundary value $\psi(1,\tau)=0$. If we let α approach zero from above, $\psi(\eta,\tau)$ will approach $\phi_0(\eta,\tau)=\eta-1$ so that $\psi_\tau(\eta,\tau)$ will become small for small α and it should also be noted that $\psi_\eta(1,\tau)=\cos(\alpha\tau)$.

REMARK 5. Integrating by parts, it is seen that the coefficients $a_0(\tau)$ and $a_1(\tau)$ of (98) can be written in the form

$$\begin{array}{c} a_1(\tau) = -\int_0^1 \left(\psi(\eta,\tau)+\eta\psi_\eta(\eta,\tau)\right) V(\eta,\tau)\mathrm{d}\eta\ , \\ a_0(\tau) = h(\tau)\psi(0,\tau) + 2\left(f(\tau)\psi_\eta(1,\tau) - g(\tau)\psi_\eta(0,\tau)\right) + \\ 2\int_0^1 \psi_\tau(\eta,\tau)V(\eta,\tau)\mathrm{d}\eta\ , \end{array} \tag{100}$$

where the last integral can be made as small as desired by choosing a sufficiently small α. Moreover, $V(\eta,\tau)$ defined in (78, 79) is bounded by either $g(\tau)$ or $f(\tau)$ through the maximum principle **[10]**. Then, we see that

$$\begin{array}{c} |a_1(\tau)| \le \max\left(f(\tau),g(\tau)\right)\int_0^1 |\psi(\eta,\tau)+\eta\psi_\eta(\eta,\tau)|\,\mathrm{d}\eta\ , \\ |a_0(\tau)| \ge \Big|\ \Big|h(\tau)\psi(0,\tau)+2\int_0^1\psi_\tau(\eta,\tau)V(\eta,\tau)\mathrm{d}\eta\Big| - \\ 2\left|f(\tau)\psi_\eta(1,\tau)-g(\tau)\psi_\eta(0,\tau)\right|\ \Big| \ \Rightarrow \\ \frac{|a_1(\tau)|}{|a_0(\tau)|} \le \frac{\max(f(\tau),g(\tau))\int_0^1|\psi(\eta,\tau)+\eta\psi_\eta(\eta,\tau)|\mathrm{d}\eta}{\Big|\ \Big|h(\tau)\psi(0,\tau)+2\int_0^1\psi_\tau(\eta,\tau)V(\eta,\tau)\mathrm{d}\eta\Big|-2|f(\tau)\psi_\eta(1,\tau)-g(\tau)\psi_\eta(0,\tau)|\ \Big|}\ . \end{array} \tag{101}$$

We now adopt $\alpha=0.1$, $f(\tau)=0$ from **[50]** and study *case I* with $h(\tau)=-\mathrm{e}^{-\tau}$ and *case II* with $h(\tau)=-\mathrm{e}^{-\frac{\tau}{2\pi}}$. For instance, in case I with $\psi(\eta,\tau)=\phi_0(\eta,\tau)=\eta-1$ we obtain the

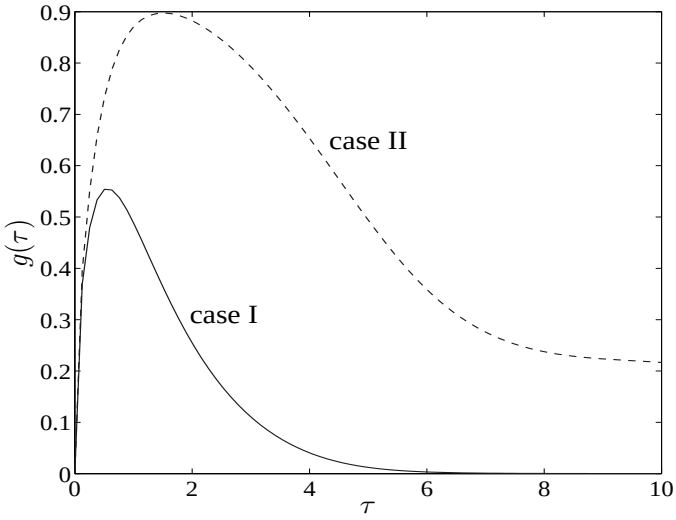

FIGURE 3.2. Errorless temperature measurements for cases I and II at the left end of the computational domain.

estimate

$$\frac{|a_1(\tau)|}{|a_0(\tau)|} \leq \frac{g(\tau)\int_0^1 |2\eta-1|\mathrm{d}\eta}{|\mathrm{e}^{-\tau}-2g(\tau)|} = \frac{g(\tau)}{2|\mathrm{e}^{-\tau}-2g(\tau)|} \ . \tag{102}$$

In Fig. 3.1 we can compare this bound with the factual value of $\left|\frac{a_1(\tau)}{a_0(\tau)}\right|$. In both of the cases I and II, $a_0(\tau)$ and $a_1(\tau)$ have opposite signs, so the differential equation (98) cannot be solved in the forward time direction due to exponential growth. For comparison, we tried in the cases I and II of this example to solve (98) backwards, as the theoretical boundary trajectory was known and, thus, an "initial value" for such a computation could be found. The result did not differ significantly from that obtained by disregarding the derivative term and using the algebraic relation $d(\tau) \approx \frac{b(\tau)}{a_0(\tau)}$.

In Figure 3.2, the "measured" temperature $g(\tau)$ at the left end of the domain is depicted for both cases I and II.

In Figures 3.3 and 3.4, the theoretical as well as the estimated boundary movements are depicted, both for the derived prediction

$$d(\tau) \approx \frac{b(\tau)}{a_0(\tau)} \ , \tag{103}$$

and for a relation corrected by the disregarded integral $I'_\tau(\tau)$, treated in Lemma 7,

$$d(\tau) \approx \frac{b(\tau) + I'_\tau(\tau)}{a_0(\tau)} \ . \tag{104}$$

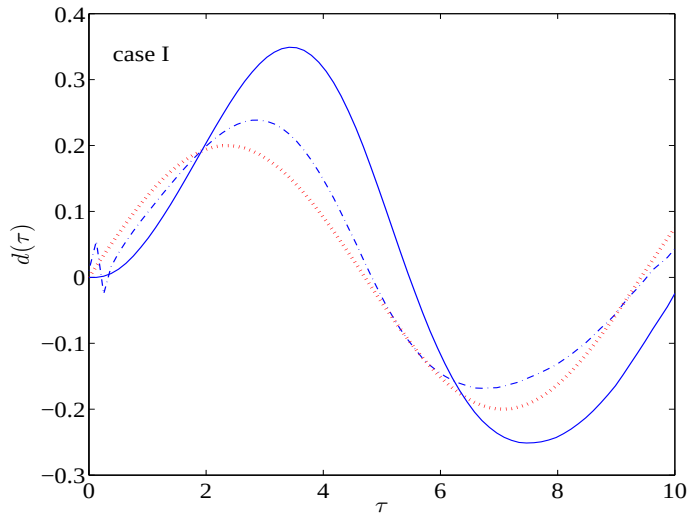

FIGURE 3.3. Theoretical boundary movement (dotted), prediction (103) (full line) as well as the corrected estimate (104) (dash-dotted) for example case I.

In a practical computation from measurements, this correction is, of course, not possible but we have included it here in an attempt to explain some of the discrepancy between our prediction and the correct theoretical value for the boundary movement $d(\tau)$.

From Figures 3.3 and 3.4 we see that a substantial part of the time lag in the prediction (103) can be explained by the omission of correction $I'_\tau(\tau)$ in (104). In case II, where the support of the measured incoming flux at the left end is larger, the estimation result is better and the correction smaller. This could also be interpreted from an information point of view, in case II there is more information (measurement signals have larger support) available for the computation than in case I and one can then also expect an improved final result.

Although this example was merely a simulation of a theoretical boundary movement, it illustrates the linearization approach and casts light on some issues raised in **[50]**, such as the question of what causes the lagging characteristics of the estimated movement. Uniqueness is not a solution property here, since the "averaging" done by using ψ causes an information loss that also results in loss of uniqueness. On the other hand, (103) does not appear to be ill-posed in any manner and stability against measurement errors can be assumed.

2. The integral equation approach

As with the linearization strategy, we start with converting to a fixed domain resulting in the equation (76)

$$\frac{1}{s^2(t)}\vartheta_{\eta\eta}(\eta,t) + \frac{\eta s'(t)}{s(t)}\vartheta_\eta(\eta,t) = \vartheta_t(\eta,t)\ , \tag{105}$$

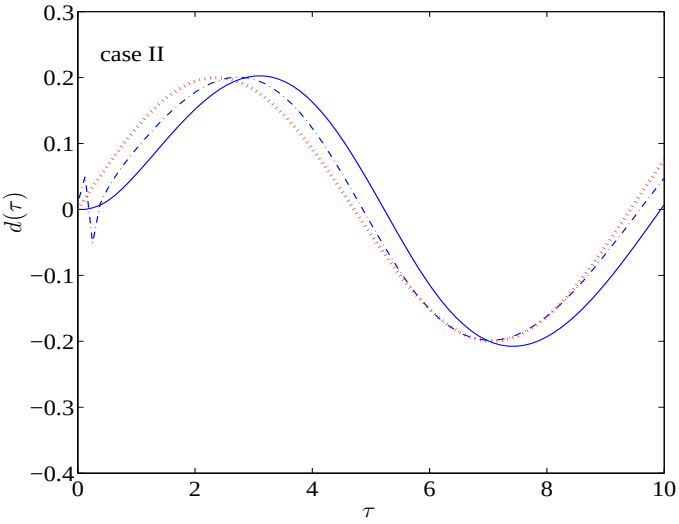

FIGURE 3.4. Theoretical boundary movement (dotted), prediction (103) (full line) as well as the corrected estimate (104) (dash-dotted) for example case II.

together with boundary conditions

$$\begin{gathered}\vartheta(0,t)=g(t)\ ,\quad \tfrac{1}{s(t)}\vartheta_\eta(0,t)=h(t)\ ,\\ \vartheta(1,t)=f(t)\ ,\quad \vartheta(\eta,0)=0\ ,\\ \eta\in[0,1],\quad t\in[0,\infty)\ ,\end{gathered}\tag{106}$$

for known piecewise continuous $f(t)$ and measured piecewise continuous $g(t)$, $h(t)$. Now, in order to simplify (105) before transferring to an integral equation formulation, we consider the new time variable through the increasing and injective function $\phi(t)$

$$\tau=\phi(t)=\int_0^t\frac{\mathrm{d}p}{s^2(p)}\tag{107}$$

and define $\omega(\eta,\tau)=\omega(\eta,\phi(t))=\vartheta(\eta,t)$. Then, denoting $m(\tau)=s'(t)s(t)$, our governing partial differential equation (105) takes the form

$$\omega_{\eta\eta}(\eta,\tau)+\eta m(\tau)\omega_\eta(\eta,\tau)=\omega_\tau(\eta,\tau)\ ,\tag{108}$$

with boundary conditions

$$\begin{gathered}\omega(0,\tau)=g\left(\phi^{-1}(\tau)\right)\ ,\quad \omega_\eta(0,\tau)=s\left(\phi^{-1}(\tau)\right)h\left(\phi^{-1}(\tau)\right)\ ,\\ \omega(1,\tau)=f\left(\phi^{-1}(\tau)\right)\ ,\quad \omega(\eta,0)=0\ ,\\ \eta\in[0,1],\quad \tau\in[0,\infty)\ .\end{gathered}\tag{109}$$

Before arriving at our integral equation formulation, we consider the following auxiliary result

THEOREM 4. *(Existence and uniqueness) For piecewise continuous* $\mathtt{f}$ *and* $\mathtt{h}$*, the finite geometry problem*

$$v_{xx}(x,t) = v_t(x,t) \ , \tag{110}$$

$$\begin{gathered} v(1,t) = \mathtt{f}(t) \ , \\ v_x(0,t) = \mathtt{h}(t) \ , \\ v(x,0) = 0 \ , \\ x \in [0,1], \quad t \in [0,\infty) \end{gathered} \tag{111}$$

has the unique solution

$$v(x,t) = \int_0^t \mathcal{K}(x,t-p)\mathtt{f}(p)\mathrm{d}p - \int_0^t \mathcal{H}(x,t-p)\mathtt{h}(p)\mathrm{d}p \ , \tag{112}$$

with

$$\begin{gathered} \mathcal{H}(x,t) = \frac{1}{\sqrt{\pi t}}\left(\mathrm{e}^{-\frac{x^2}{4t}} + \sum_{n=1}^{\infty}(-1)^n \mathrm{e}^{-\frac{(2n+x)^2}{4t}} + \sum_{n=1}^{\infty}(-1)^n \mathrm{e}^{-\frac{(2n-x)^2}{4t}}\right) = \\ \sum_{n=-\infty}^{\infty}(-1)^n \mathcal{I}(x+2n,t) \ , \end{gathered}$$

$$\begin{gathered} \mathcal{K}(x,t) = \frac{1}{2\sqrt{\pi t^3}}\left((1+x)\mathrm{e}^{-\frac{(1+x)^2}{4t}} + \sum_{n=1}^{\infty}(-1)^n(2n+1+x)\mathrm{e}^{-\frac{(2n+1+x)^2}{4t}} + \right. \\ \left. (1-x)\mathrm{e}^{-\frac{(1-x)^2}{4t}} + \sum_{n=1}^{\infty}(-1)^n(2n+1-x)\mathrm{e}^{-\frac{(2n+1-x)^2}{4t}}\right) = \\ \sum_{n=0}^{\infty}(-1)^n \left(\mathcal{I}_x(2n+1+x,t) + \mathcal{I}_x(2n+1-x,t)\right) \ , \end{gathered} \tag{113}$$

where $\mathcal{I}(x,t) = \frac{\mathrm{e}^{-\frac{x^2}{4t}}}{\sqrt{\pi t}}$.

Proof. A proof can be furnished along the same lines as for Theorem 6.3.1. in Cannon [**10**], whence uniqueness is completely analogous. See also the comments in conjunction with Theorem 1 and remark 1; similar observations can be made here. We now construct a solution using the Laplace transform, assuming that v, $\mathtt{f}$ and $\mathtt{h}$ are exponentially bounded so that the transforms exist [**39**]. Denoting Laplace transforms with capital letters, we can consider (110, 111) in the frequency space as the boundary value problem

$$\mathsf{V}_{xx}(x,\mathsf{p}) = \mathsf{p}\mathsf{V}(x,\mathsf{p}) \ , \tag{114}$$

$$\begin{gathered} \mathsf{V}(1,\mathsf{p}) = \mathtt{F}(\mathsf{p}) \ , \\ \mathsf{V}_x(0,\mathsf{p}) = \mathtt{H}(\mathsf{p}) \ . \end{gathered} \tag{115}$$

It is a routine task to solve (114, 115) and the solution turns out to be

$$\begin{gathered} \mathsf{V}(x,\mathsf{p}) = \mathtt{F}(\mathsf{p})\frac{\mathrm{e}^{x\sqrt{\mathsf{p}}}+\mathrm{e}^{-x\sqrt{\mathsf{p}}}}{\mathrm{e}^{\sqrt{\mathsf{p}}}+\mathrm{e}^{-\sqrt{\mathsf{p}}}} + \frac{\mathtt{H}(\mathsf{p})}{\sqrt{\mathsf{p}}}\ \frac{\mathrm{e}^{(x-1)\sqrt{\mathsf{p}}}-\mathrm{e}^{(1-x)\sqrt{\mathsf{p}}}}{\mathrm{e}^{\sqrt{\mathsf{p}}}+\mathrm{e}^{-\sqrt{\mathsf{p}}}} = \\ \mathtt{F}(\mathsf{p})\frac{\mathrm{e}^{(x-1)\sqrt{\mathsf{p}}}+\mathrm{e}^{-(x+1)\sqrt{\mathsf{p}}}}{1+\mathrm{e}^{-2\sqrt{\mathsf{p}}}} + \frac{\mathtt{H}(\mathsf{p})}{\sqrt{\mathsf{p}}}\ \frac{\mathrm{e}^{(x-2)\sqrt{\mathsf{p}}}-\mathrm{e}^{-x\sqrt{\mathsf{p}}}}{1+\mathrm{e}^{-2\sqrt{\mathsf{p}}}} \ . \end{gathered} \tag{116}$$

In order to obtain a solution applicable for small times, we use the asymptotic series for the denominator in (116)

$$\left(1+\mathrm{e}^{-2\sqrt{\mathsf{p}}}\right)^{-1} = \sum_{n=0}^{\infty}(-1)^n \mathrm{e}^{-2n\sqrt{\mathsf{p}}} \ . \tag{117}$$

Inserting (117) into (116) yields

$$
\begin{array}{r}
\mathsf{V}(x,\mathsf{p}) = \mathsf{F}(\mathsf{p})\left(\sum_{n=0}^{\infty}(-1)^n \mathrm{e}^{(x-2n-1)\sqrt{\mathsf{p}}} + \sum_{n=0}^{\infty}(-1)^n \mathrm{e}^{(-x-2n-1)\sqrt{\mathsf{p}}}\right) + \\
\frac{\mathsf{H}(\mathsf{p})}{\sqrt{\mathsf{p}}}\left(\sum_{n=0}^{\infty}(-1)^n \mathrm{e}^{(x-2n-2)\sqrt{\mathsf{p}}} - \sum_{n=0}^{\infty}(-1)^n \mathrm{e}^{(-x-2n)\sqrt{\mathsf{p}}}\right) = \\
\mathsf{F}(\mathsf{p})\left(\sum_{n=0}^{\infty}(-1)^n \mathrm{e}^{-(2n+1+x)\sqrt{\mathsf{p}}} + \sum_{n=0}^{\infty}(-1)^n \mathrm{e}^{-(2n+1-x)\sqrt{\mathsf{p}}}\right) - \\
\frac{\mathsf{H}(\mathsf{p})}{\sqrt{\mathsf{p}}}\left(\mathrm{e}^{-x\sqrt{\mathsf{p}}} + \sum_{n=1}^{\infty}(-1)^n \mathrm{e}^{-(x+2n)\sqrt{\mathsf{p}}} + \sum_{n=1}^{\infty}(-1)^n \mathrm{e}^{-(2n-x)\sqrt{\mathsf{p}}}\right) \ .
\end{array}
\tag{118}
$$

Inverting the Laplace transforms now leads to the convolution (112) with kernels given by (113). Uniqueness follows from the extended uniqueness Theorem 1.6.6. in Cannon [**10**], or alternatively by applying the energy method (section 6.4. in [**10**]). □

Revisiting (108, 109), we observe that the second term on the left hand side in (108) may be disregarded and the results of Theorem 4 can be put to work if $m(\tau) \approx 0$, i.e., if the boundary movement is slow and $s'(t) \approx 0$. In such case, we obtain an approximate integral formulation for the solution to (108, 109) from (112) according to

$$
\begin{array}{rcl}
\omega(\eta,\tau) & \approx & \int_0^\tau \mathcal{K}(\eta,\tau-p) f\left(\phi^{-1}(p)\right) \mathrm{d}p \\
& - & \int_0^\tau \mathcal{H}(\eta,\tau-p) s\left(\phi^{-1}(p)\right) h\left(\phi^{-1}(p)\right) \mathrm{d}p \ .
\end{array}
\tag{119}
$$

Evaluating (119) at $\eta = 0$, considering the boundary condition $\omega(0,\tau) = g\left(\phi^{-1}(\tau)\right)$ in (109) leads to an approximate integral equation for the boundary function $\phi(\tau)$, defined in (107).

$$
\begin{array}{rcl}
g\left(\phi^{-1}(\tau)\right) & \approx & \int_0^\tau \mathcal{K}(0,\tau-p) f\left(\phi^{-1}(p)\right) \mathrm{d}p \\
& - & \int_0^\tau \mathcal{H}(0,\tau-p) s\left(\phi^{-1}(p)\right) h\left(\phi^{-1}(p)\right) \mathrm{d}p \ .
\end{array}
\tag{120}
$$

Noting that (107) gives $t = \phi^{-1}(\tau)$ and changing the integration variable to $q = \phi^{-1}(p)$ simplifies (120) to

$$
\begin{array}{rcl}
g(t) & \approx & \int_0^t \mathcal{K}(0,\phi(t)-\phi(q)) f(q)\phi'(q) \mathrm{d}q \\
& - & \int_0^t \mathcal{H}(0,\phi(t)-\phi(q)) h(q)\sqrt{\phi'(q)} \mathrm{d}q \ .
\end{array}
\tag{121}
$$

The objective is now to solve (121) for the function $\phi(t)$ with known piecewise continuous functions f, g and h. This enables us to recover the boundary movement from (107) through the relation $s(t) = \frac{1}{\sqrt{\phi'(t)}}$. Before outlining a finite difference discretization for the numerical solution procedure, we give some general remarks on existence after noting that the kernels in (121) can be expressed compactly as

$$
\begin{array}{c}
\mathcal{H}_0(t) := \mathcal{H}(0,t) = \frac{1}{\sqrt{\pi t}}\left(1 + 2\sum_{n=1}^{\infty}(-1)^n \mathrm{e}^{-\frac{n^2}{t}}\right) =: \frac{\mathcal{H}_p(t)}{\sqrt{t}} \ , \\
\mathcal{K}_0(t) := \mathcal{K}(0,t) = \frac{1}{2\sqrt{\pi t^3}}\left(\mathrm{e}^{-\frac{1}{4t}} + 2\sum_{n=1}^{\infty}(-1)^n (2n+1) \mathrm{e}^{-\frac{(2n+1)^2}{4t}}\right) \ .
\end{array}
\tag{122}
$$

Remark 6. (Existence and uniqueness) The integral equation (121) is a nonlinear Volterra equation of the first kind. Note that the kernel $\mathcal{H}_0(t)$ blows up in the limit $t \downarrow 0$, due to the constant in the first parenthesis of (122). This makes investigation of existence and smoothing properties complicated. Note that the first integral in (121) is exact and well-behaved for bounded, piecewise continuous input data f and that $\mathcal{K}_0(t)$ is bounded as $t \downarrow 0$. The second integral, however, is problematic due to the singularity of $\mathcal{H}_0(t)$ at the origin and the presence of the factor $\sqrt{\phi'(t)}$. Without auxiliary constraints on the boundary position $s(t)$ in (107),

this factor is not bounded. A possible existence result for ϕ of (121) is likely to require at least boundedness for ϕ'. The singularity of $\mathcal{H}_0(t)$ at the origin could be handled by splitting the integration interval in (121) into two parts, yielding a small interval close to t where $\phi'(q) \approx (\phi(t) - \phi(q))(t-q)^{-1}$ is an approximation to the desired accuracy. In this interval, keeping in mind (122), the second integral will resemble that of a nonlinear Abel integral equation [**1**]. Further requirements for investigating existence are boundedness and piecewise continuity of the input data h and differentiation of $g(t)$ on the left hand side of (121) in some suitable sense.

REMARK 7. (Discretization) In a practical computation the integral equation must be solved numerically and to do this, we recall (122) and split the kernel into two parts according to

$$\begin{aligned} \mathcal{H}_0(t) &= \tfrac{1}{\sqrt{\pi t}} + \mathcal{H}_1(t) \ , \\ \mathcal{H}_1(t) &= \tfrac{2\sum_{n=1}^{\infty}(-1)^n \mathrm{e}^{-\frac{n^2}{t}}}{\sqrt{\pi t}} \ . \end{aligned} \tag{123}$$

Now, consider the integral equation (121) in the form

$$\begin{gathered} g(t) \approx \int_0^{t-\Delta t} \mathcal{K}_0(\phi(t)-\phi(q)) f(q)\phi'(q)\mathrm{d}q - \tfrac{1}{\sqrt{\pi}} \int_{t-\Delta t}^{t} \tfrac{h(q)\sqrt{\phi'(q)}\mathrm{d}q}{\sqrt{\phi(t)-\phi(q)}} - \\ \int_{t-\Delta t}^{t} \left[\mathcal{H}_1(\phi(t)-\phi(q))h(q)\sqrt{\phi'(q)} - \mathcal{K}_0(\phi(t)-\phi(q))f(q)\phi'(q) \right] \mathrm{d}q - \\ \int_0^{t-\Delta t} \mathcal{H}_0(\phi(t)-\phi(q))h(q)\sqrt{\phi'(q)}\mathrm{d}q \ , \end{gathered} \tag{124}$$

where Δt was introduced as a means of handling the singularity of $\mathcal{H}_0(t)$ at the origin. The contribution from the integral involving $\mathcal{H}_1(t)$ and $\mathcal{K}_0(t)$ over $(t-\Delta t, t)$ can be shown to be small for a sufficiently small $\Delta t > 0$. A norm bound on this integral may be imposed in order to obtain a criterion for the choice of Δt.

Discretize the first form of (124) without regularization and with the integral involving $\mathcal{H}_1$ disregarded

$$\begin{gathered} g(t) + \tfrac{1}{\sqrt{\pi}} \int_{t-\Delta t}^{t} \tfrac{h(q)\mathrm{d}q}{\sqrt{t-q}} \approx \\ \int_0^t \mathcal{K}_0(\phi(t)-\phi(q)) f(q)\phi'(q)\mathrm{d}q - \int_0^{t-\Delta t} \mathcal{H}_0(\phi(t)-\phi(q))h(q)\sqrt{\phi'(q)}\mathrm{d}q \end{gathered} \tag{125}$$

on the interval $[0,t]$ on the grid $(t_i)_{i=0}^M = 0, \Delta t, 2\Delta t, \cdots, M\Delta t$. If we discretize the solution ϕ on the same grid and denote the gridpoint values by $\phi_0, \phi_1, \phi_2, \cdots, \phi_M$ we have from (107) $\phi_0 = 0$ and $\phi_M = \phi(t)$. Furthermore, since $\phi'(0) = s^{-2}(0)$ we can extrapolate $\phi_1 = \Delta t \phi'(0) = \frac{\Delta t}{s^2(0)}$. The discrete trapezoidal rule approximation to (125) is thus

$$\begin{gathered} g(t_M) + \tfrac{1}{\sqrt{\pi}} \int_{t_{M-1}}^{t_M} \tfrac{h(q)\mathrm{d}q}{\sqrt{t_M - q}} \approx \\ \tfrac{\Delta t}{2} \tfrac{\mathcal{K}_0(\phi_M) f(0)}{s^2(0)} + \sum_{i=1}^{M-1} \mathcal{K}_0(\phi_M - \phi_i) f(t_i)(\phi_{i+1} - \phi_{i-1})/2 - \\ \tfrac{\Delta t}{2} \tfrac{\mathcal{H}_0(\phi_M) h(0)}{s(0)} - \sum_{i=1}^{M-2} \mathcal{H}_0(\phi_M - \phi_i) h(t_i) \sqrt{\Delta t(\phi_{i+1} - \phi_{i-1})/2} - \\ \tfrac{1}{2} \mathcal{H}_0(\phi_M - \phi_{M-1}) h(t_{M-1}) \sqrt{\Delta t(\phi_M - \phi_{M-2})/2} \ . \end{gathered} \tag{126}$$

To compute $\phi(t)$ we need to solve the nonlinear algebraic equation (126) for ϕ_M with $M = 2, 3, \cdots$ in order to obtain a function value at each gridpoint.

Since $\phi(t)$ is an increasing function, all terms in (126) are defined and the solution for each ϕ_M lies in the interval (ϕ_{M-1}, ∞). We also observe that $\mathcal{H}_0(\phi_M - \phi_{M-1})$ blows up in

the limit $\phi_M \to \phi_{M-1}$. The temperatures at the left and right end of the domain, $g(t)$ and $f(t)$, respectively, as well as the left-end flux $h(t)$, are restricted only by compatibility with the solution field. We will elaborate further on this requirement later. This means that they should be consistent with the solution to (105, 106) for a known boundary trajectory $s(t)$. Hence, any general conclusions as to the existence and uniqueness of the solution ϕ_M to (126) cannot be drawn.

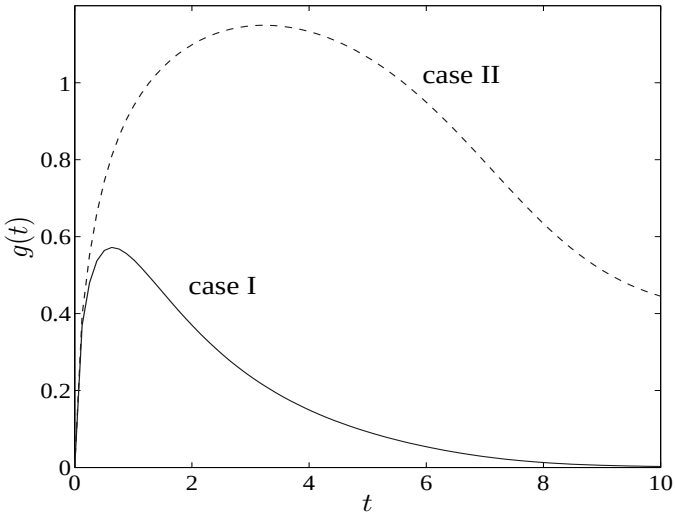

FIGURE 3.5. Errorless temperature measurements at the left end of the computational domain for cases I and II and boundary movement $s_b(t) = 0.7\sin\frac{t}{2} + \mathrm{e}^{\frac{t}{10}}$.

We proceed with an example, illustrating the solution procedure as well as the boundary movement estimation performance for moderate boundary variation and for a case where the assumption $s'(t) \approx 0$ leading to (119) is violated.

EXAMPLE 4. Consider errorless data $f(t)$, $g(t)$, $h(t)$ in (106) and a theoretical boundary movement described by $s_a(t) = 1+0.2\sin\left(\frac{2t}{3}\right)$ and, alternatively, $s_b(t) = 0.7\sin\frac{t}{2}+\mathrm{e}^{\frac{t}{10}}$ adopted from **[50]**. Note that the latter boundary trajectory violates the assumption of slow boundary movement. As in example 3 of the previous section, we adopt $f(t) = 0$ from **[50]** and study *case I* with $h(t) = -\mathrm{e}^{-t}$ and *case II* with $h(t) = -\mathrm{e}^{-\frac{t}{2\pi}}$. For $s_b(t)$, the measurements are depicted in Figure 3.5 and for the boundary variation $s_a(t)$, the function $g(t)$ can be computed as in example 3 by solving the direct problem and extracting the temperature at the left end of the domain, c.f. Figure 3.2. The result for $s_a(t)$ in cases I and II is depicted in Figure 3.7 and the result for $s_b(t)$ in cases I and II in Figure 3.8.

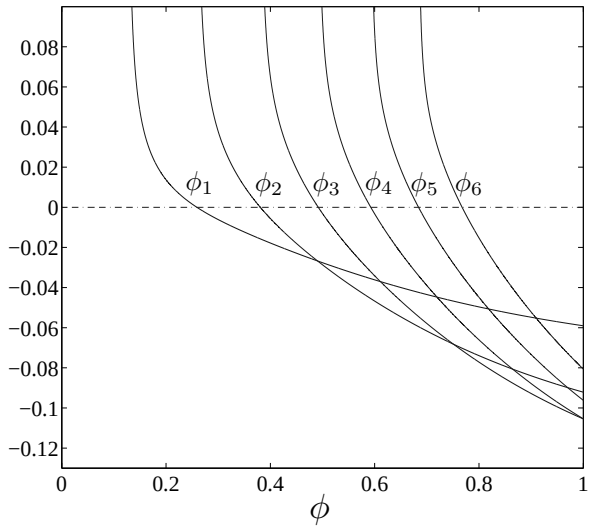

FIGURE 3.6. The first six zero points ϕ_M in the solution of the nonlinear algebraic equation (126) for Case I and $s_b(t)$.

The task is now to solve the the nonlinear algebraic equation (126) according to the procedure described in remark 7. For this, we adopt the time step $\Delta t = 2^{-3}$. As a curiosity, we note that the integral on the left hand side of (126) can here be computed according to

$$\frac{1}{\sqrt{\pi}} \int_{t_{M-1}}^{t_M} \frac{h(q)\mathrm{d}q}{\sqrt{t_M - q}} = \begin{cases} i\mathrm{erf}(i\sqrt{\Delta t})\mathrm{e}^{-t_M} \ , & \text{Case I} \\ i\sqrt{2\pi}\mathrm{erf}(i\sqrt{\frac{\Delta t}{2\pi}})\mathrm{e}^{-\frac{t_M}{2\pi}} \ , & \text{Case II} \ . \end{cases} \tag{127}$$

We used the Faddeeva function [**40**] to calculate the appropriate function values for the complex error function in (127).

An illustration of the solution to (126) is given in Figure 3.6, for Case I ($h(t) = -\mathrm{e}^{-t}$) and theoretical boundary trajectory $s_b(t) = 0.7 \sin \frac{t}{2} + \mathrm{e}^{\frac{t}{10}}$. The difference between the left- and right-hand sides of the equation is depicted for $M = 1, \ldots, 6$. The point, where each curve changes sign corresponds to the solution ϕ_M.

As described in remark 7, we can obtain the gridpoint values for the increasing function $\phi(t)$ in this way and the boundary trajectory $s(t)$ can be obtained from these through the relation (107) giving $\phi'(t) = s^{-2}(t)$.

The result of this for Cases I and II as well as for the theoretical boundary trajectories $s_a(t)$ and $s_b(t)$ is depicted in Figures 3.7 and 3.8. We observe that the estimation performance for $s_a(t)$ is good in both cases I and II. Moreover, also for $s_b(t)$, we get satisfactory agreement between our estimate and the theoretical movement, although the assumption of moderate variation is invalid. Apparently, case II with a larger support for the function $h(t)$ gives

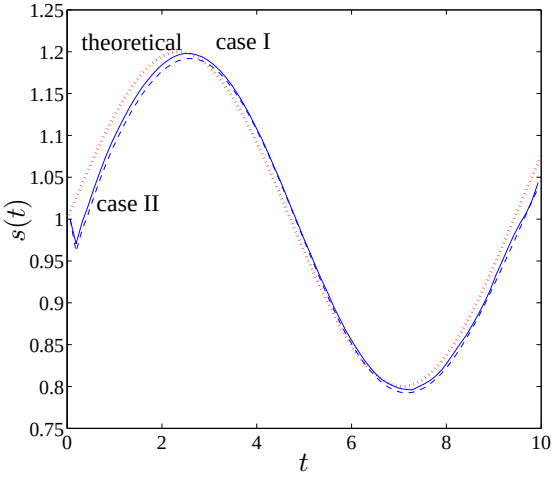

FIGURE 3.7. Theoretical boundary trajectory $s_a(t) = 1+0.2\sin\left(\frac{2t}{3}\right)$ (dotted) and computed estimates for Case I ($h(t) = -\mathrm{e}^{-t}$) (full line) and Case II ($h(t) = -\mathrm{e}^{-\frac{t}{2\pi}}$) (dashed).

somewhat poorer performance than case I, in contrast to the results for the linearization approach presented in the previous section.

Based on remark 7, we can presume the computation to be severely ill-posed. Figure 3.6 appears to confirm this, as the first gridpoint value for ϕ is determined by the curve having the zero-point ϕ_1 in the graph. A small perturbation to this curve shifts the zero significantly, which in turn affects the following zeros as each curve is functionally dependent on the previous one. This is a characteristic of the higher zeros as well, rendering the gridpoint value computation for ϕ strongly sensitive to noise in the data for $f(t)$, $g(t)$, $h(t)$. In addition, to obtain the final result, we need to differentiate ϕ to obtain $s(t)$ from the relation (107), which in itself is an ill-posed operation.

3. The sideways heat conduction eq. and boundary identification

3.1. Preliminaries. As previously indicated, in conjunction with (74, 75), solution of the sideways heat conduction equation can be applied to boundary identification. The basic idea is to consider a finite time domain through discretization and to solve the associated vector-valued Cauchy problem for a spatial region, e.g., as in the Euler "space marching" scheme (66). With a suitably chosen formulation and a bounded approximation to the time differentiation operator, reasonable results can be achieved with a fairly simple algorithm to a low computational cost. As limitations, however, we have observed poor performance of the method when a large estimated trajectory $s(t)$ is combined with low flux $h(t)$. Thus, when we attempted computation of the example of the previous section, this method failed to produce acceptable results. This is an expected behavior, since it means that the method breaks down

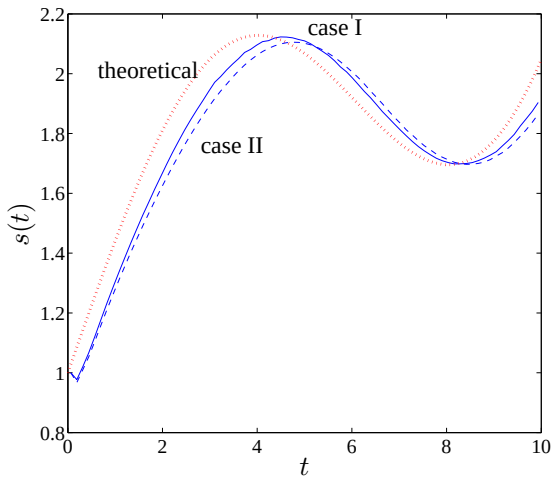

FIGURE 3.8. Theoretical boundary trajectory $s_b(t) = 0.7 \sin \frac{t}{2} + \mathrm{e}^{\frac{t}{10}}$ (dotted) and computed estimates for Case I ($h(t) = -\mathrm{e}^{-t}$) (full line) and Case II ($h(t) = -\mathrm{e}^{-\frac{t}{2\pi}}$) (dashed).

when estimation distance grows and the data is blurred out. Fortunately, this characteristic does not play a significant role in the applications /**I-IX**/ we are concerned with here.

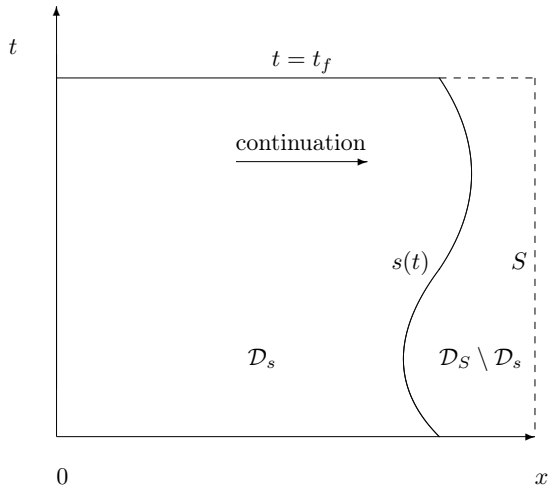

FIGURE 3.9. The relation between domains for the classical sideways diffusion problem and the boundary identification problem for a finite time horizon.

3.2. Remarks on existence and uniqueness. Consider now the situation depicted in the (x,t)-plane in Fig. 3.9 for (74, 75) having a moving boundary $s(t) > 0$ and a specified solution function on this boundary, i.e., $v(s(t),t) = f(t)$. The objective is to compute the function $s(t)$ in

$$v_{xx}(x,t) = v_t(x,t) \ , \tag{128}$$

$$\begin{array}{c} v(0,t) = g(t) \ , \quad v_x(0,t) = h(t) \ , \\ v(s(t),t) = f(t) \ , \quad v(x,0) = 0 \ , \\ x \in [0,s(t)], \quad t \in [0,t_f] \ , \end{array} \tag{129}$$

from measured $g(t) \in C^1([0,t_f])$, $h(t) \in C^1([0,t_f])$ and known $f(t) \in C^1([0,t_f])$. A solution need not exist for all such data, however, as we can see from the following.

Counterexample 2. (Existence) Consider the input

$$\begin{array}{c} v(0,t) = g(t) = 1 - \mathrm{e}^{-t} \ , \quad v_x(0,t) = h(t) = -\mathrm{e}^{-t} \ , \\ v(s(t),t) = f(t) = 2 \ , \quad t \in [0,t_f] \ . \end{array} \tag{130}$$

It is not hard to see that there does not exist a solution $s(t)$, compatible with these data, although the data are valid initial and boundary conditions for our problem.

Clearly, existence of a solution requires *compatibility* of the data, in this sense: These have such properties that any two functions of $g(t)$, $h(t)$ and $f(t)$ together with the solution $s(t)$ specify the third one of those functions through the solution of a direct problem. This direct problem can be formulated by (108, 109), which essentially can be written in the form given in Theorem 20.3.3. of **[10]**. It can be routinely checked that such a direct problem satisfies the conditions for existence and uniqueness of the third function under the assumptions made here.

Lemma 8. *(Uniqueness) The solution $s(t)$ to the boundary identification problem, with data subject to the above restrictions and the requirement* $\sup_{0<t<t_f} g(t) < \sup_{0<t<t_f} f(t) > 0$, *is unique if it exists.*

Proof. Assume there exists two solutions $s_1(t)$ and $s_2(t)$ corresponding to the same function $f(t)$ in (129) according to the situation depicted in Fig. 3.10. Then, both $\mathcal{D}_s$ and $\mathcal{D}_s \cup \mathcal{D}_{ss}$ constitutes the domain of a parabolic PDE and the solution $v(x,t)$ thereof has the value $f(t)$ on both $s_1(t)$ and $s_2(t)$. In this case, the maximum of $v(x,t)$ on $\mathcal{D}_s \cup \mathcal{D}_{ss}$ would occur on both $s_2(t)$ and at an interior point $s_1(t)$. For this parabolic PDE, the strong maximum principle (Theorem 15.3.1. of **[10]**) is valid, implying that $v(x,t)$ is constant. This contradicts the assumptions and brings us to the conclusion $s_1(t) = s_2(t)$. □

3.3. The Cauchy-problem. As in our previous approach to the sideways heat equation, we can consider (128, 129) as a Cauchy-problem in the spatial variable x:

$$\left[\begin{array}{c} v(t) \\ v_x(t) \end{array} \right]_x (x) \quad = \quad \left[\begin{array}{cc} 0 & I \\ \frac{\partial}{\partial t} & 0 \end{array} \right] \left[\begin{array}{c} v(t) \\ v_x(t) \end{array} \right] (x) \tag{131}$$

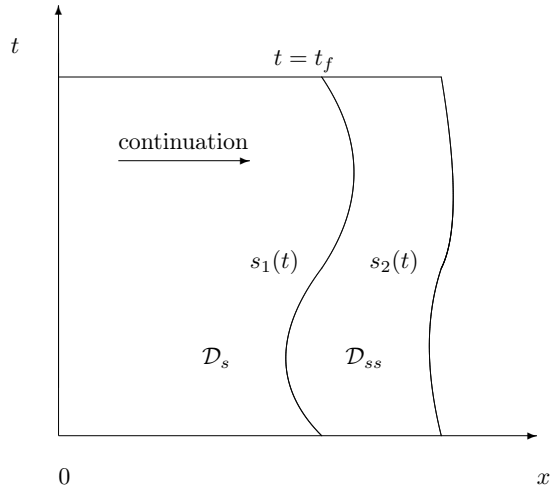

FIGURE 3.10. The boundary identification problem for a situation with solution non-uniqueness.

with the "initial" condition and known state at $t = 0$ and on the boundary, according to

$$\begin{gathered} \left[\begin{array}{c} v(t) \\ v_x(t) \end{array} \right] (0) = \left[\begin{array}{c} g(t) \\ h(t) \end{array} \right] , \\ v(s(t),t) = f(t) \ , \quad v(x,0) = 0 \ , \\ x \in [0, s(t)], \quad t \in [0, t_f], \ . \end{gathered} \tag{132}$$

The objective of boundary identification is to find $s(t)$ and, as previously stated, this can be done by solving (131, 132) as an initial value problem in the variable x. Then, the time-varying functions are represented by vectors consisting of function values at sampled times and the operator matrix on the right-hand-side of (131) by a discrete approximation. We have observed that this operator matrix is unbounded, making it necessary to consider such an approximation carefully in order to preserve numerical stability in computations. We will return to this issue later. Letting the vectors $\mathbf{v}(x)$ and $\mathbf{v}_x(x)$ approximate $v(x,t)$ and $v_x(x,t)$, respectively, and considering null matrices $\mathbf{0}$ as well as the identity matrix $\mathbf{I}$ and the matrix $\mathbf{D}$ containing a stable discrete approximation to the operator $\frac{\partial}{\partial t}$, we have the system of ordinary differential equations

$$\left[\begin{array}{c} \mathbf{v} \\ \mathbf{v}_x \end{array} \right]_x (x) \quad = \quad \left[\begin{array}{c|c} \mathbf{0} & \mathbf{I} \\ \hline \mathbf{D} & \mathbf{0} \end{array} \right] \left[\begin{array}{c} \mathbf{v} \\ \mathbf{v}_x \end{array} \right] (x) \tag{133}$$

for the transposed vector and final time t_f

$$\mathbf{v}(x) = [v(x,0) \ v(x,\Delta t) \ \cdots \ v(x, t_f - \Delta t) \ v(x,t_f)]^T \ . \tag{134}$$

The initial condition vector is formed from sampled values of $g(t)$ and $h(t)$ in (132):

$$\left[\begin{array}{c} \mathbf{v} \\ \mathbf{v}_x \end{array} \right] (0) = \left[\begin{array}{c} \mathbf{g} \\ \hline \mathbf{h} \end{array} \right] \ . \tag{135}$$

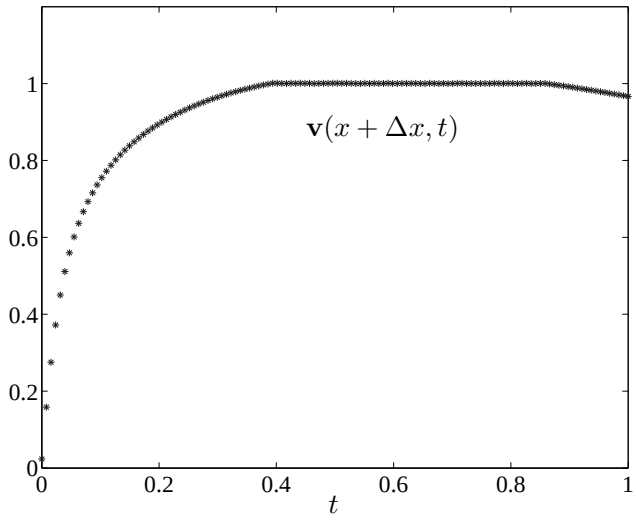

FIGURE 3.11. The elements of the vector $\mathbf{v}$ at an intermediate state during solution of (133, 135) for the case with unit state on the boundary ($f(t) = 1$ in (132)). The nodes on the middle, right-hand-side have reached the boundary state.

This system, (133, 135), can be integrated using a standard routine for systems of ODE's in a nonstandard way. Note also that the finite-difference representation $\mathbf{D}$ in (133) of the differential operator in principle requires the final-time values for the part $\mathbf{v}$ of the solution vector. However, this requirement can be circumvented by an extrapolation strategy suggested by Eldén [**20**]. During each step of the integration, we record the "distance integrated" x from the data $g(t)$, $h(t)$ at $x = 0$ and check each element of the vector $\mathbf{v}(x)$ against the corresponding value of the known state $f(t)$ on the boundary. Hence, in each step, if the boundary state has been reached, we conclude that the integrated distance gives the boundary coordinate $s(t)$ at the specific time corresponding to the particular element of the vector $\mathbf{v}(x)$. An example of this is illustrated in Fig. 3.11, where the elements in the middle have reached the state $f(t) = 1$ at the current point of the integration. After completing the integration for all elements, we obtain a vector approximation to the function $s(t)$.

REMARK 8. As previously noted, the described method performs poorly when a large estimated trajectory $s(t)$ is combined with low flux $h(t)$. Looking at (133, 135) this can be expected, as a low flux means small elements of the vector $\mathbf{h}$ which in turn yields small contributions to $\mathbf{v}(x)$ and $\mathbf{v}_x(x)$ that eventually are blurred out by the ill-posed numerical properties in the steps of the integration.

In the following, we will look at how to choose the matrix $\mathbf{D}$ in (133).

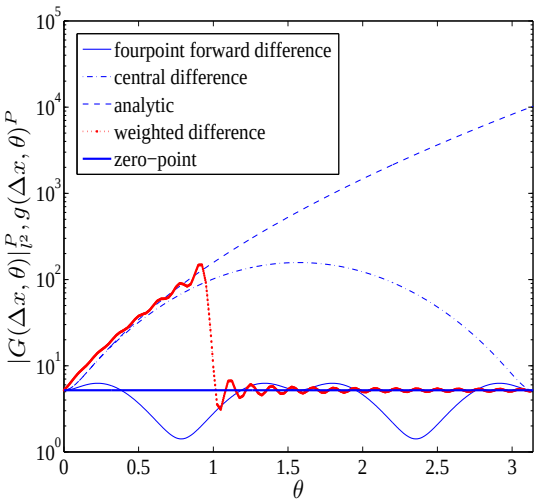

FIGURE 3.12. Amplification factors for the analytical case, two-point central (S3 in [**13**]), four-point forward and weighted difference approximations (136).

3.4. Stability; a bounded approximation to the time-differentiation operator. This issue is closely related to the discretization viewpoints given previously in conjunction with regularization of the sideways heat equation. The unbounded time-differentiation operator makes our solution of the boundary identification problem ill-posed, resulting in uncontrolled amplification of high-frequency noise present in input data. Therefore, we are interested in using an approximation that is bounded and hence less ill-posed, in the sense that amplification of high-frequency disturbances is limited, preferably in such a manner that we can specify a cutoff-frequency above which disturbances are mollified. This is not possible with a simple finite-difference approximation to $\frac{\partial}{\partial t}$. Then, the matrix $\mathbf{D}$ is a simple band matrix with most elements consisting of zeros and the amplification matrix $G(\theta)$ like (68) for a four-step forward difference approximation. From Figure 2.1, amplification factors for such finite-difference stencils appear to be low in the high-frequency range. However, in comparison with the amplification for the analytic solution, there appears to be differences in the low-frequency domain as well. When dealing with a well-posed solution, such a discrepancy can always be compensated by increasing accuracy and lowering the time step, i.e., the mesh size of the discretization. Unfortunately, as observed in the above discussion of discretization with our ill-posed solution, such a measure is counterproductive as this has a non-regularizing effect. Therefore, we will attempt to find a matrix $\mathbf{D}$, which results in an amplification as close as possible to the analytic case up to some chosen cutoff-frequency. Above this cutoff-frequency, we wish to minimize amplification in order to stabilize the computation. We will see that this can indeed be accomplished, although at the expense of loosing the sparse, banded structure of $\mathbf{D}$, present with our previous simple finite-difference stencils.

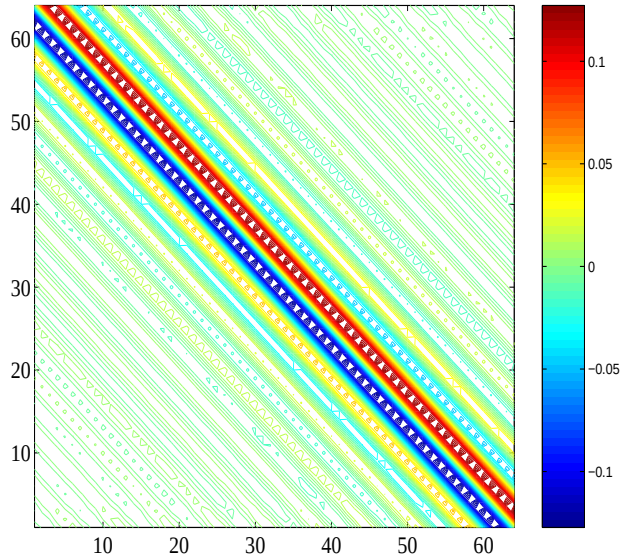

FIGURE 3.13. Contour plot for the quadratic matrix $\mathbf{D}$ (of dimension 2^6) computed with the weighted difference approximation to $\frac{\partial}{\partial t}$ appearing on the second row, first column of (136). As seen from the illustrated numerical magnitudes of the entries, the matrix is full, however reminiscent of the banded structures present in previous simpler finite difference approximations. The entries on the upper diagonal are positive while those on the lower diagonal are negative.

Consider the new amplification matrix, with the above objectives,

$$G(\theta) = \begin{bmatrix} 1 & \Delta x \\ \frac{\Delta x}{\Delta t} \sum_{n=-N}^{N} a_n \mathrm{e}^{ni\theta} & 0 \end{bmatrix}. \tag{136}$$

The idea is now to determine the finite set of coefficients $(a_n)_{n=-N}^{N}$ meeting our objective. We are working with a finite set, as these coefficients will eventually make up the entries in each row of $\mathbf{D}$. Essentially, this strategy is equivalent to computing a trigonometric polynomial approximation of $\frac{\partial}{\partial t}$ in frequency space (i.e., the ramp function) up to the cutoff-frequency. A similar approach has been used in finite-difference approximations to well-posed problems for increasing solution accuracy in the high-frequency range [**47**].

For comparison, amplification factors computed according to the Lax-Richtmyer theory [**42, 13**], introduced above from (66) onwards, are shown in Figure 3.12. For lucidity, a cutoff-frequency equal to 1 was used in this computation and we may expect favorable stability properties with respect to high-frequency noise in input data.

Similarly to our previous discussion of regularization and discretization for the sideways heat equation, the discretized solution operator of (133) can be viewed as the mapping from the noisy sensor data to the unknown boundary. The system (133), can hence be considered as a space marching scheme

$$\begin{aligned} \begin{bmatrix} \mathbf{v} \\ \mathbf{v}_x \end{bmatrix}(x+\Delta x) &= \left(\Delta x \left[\begin{array}{c|c} \mathbf{0} & \mathbf{I} \\ \hline \mathbf{D} & \mathbf{0} \end{array}\right] + \mathbf{I}\right) \begin{bmatrix} \mathbf{v} \\ \mathbf{v}_x \end{bmatrix}(x) \\ &:= C(\Delta x, \Delta t) \begin{bmatrix} \mathbf{v} \\ \mathbf{v}_x \end{bmatrix}(x) \end{aligned} \tag{137}$$

Introducing the Fourier image $G(\Delta x, \theta)$, in terms of the normalized frequency θ, of $C(\Delta x, \Delta t)$, one has the relation

$$\|C^P\| = \max_{0 \le \theta \le \pi} |G(\theta)^P|_{l^2}, \tag{138}$$

where $\|\cdot\|$ denotes the L^2 norm in the time variable, $|\cdot|_{l^2}$ the Euclidean norm and P is the maximum number of spatial steps required to reach the desired boundary. The matrix $G(\theta)$ is now the 2×2 amplification matrix (136). For comparison, the corresponding analytical solution operator for one space step Δx is a convolution kernel with the Fourier image $\mathrm{e}^{\Delta x \sqrt{i\theta/\Delta t}}$. The magnitude of this is $g(\Delta x, \theta) = \mathrm{e}^{\Delta x \sqrt{|\theta|/2\Delta t}}$ to which $|G(\Delta x, \theta)|_{l^2}$ is a discrete approximation. Thus, marching the input data P spatial steps to reach the desired boundary amplifies the noise by a factor $g(\Delta x, \theta)^P$. Alternative discretizations, also discussed here briefly in conjunction with the sideways heat equation, are treated extensively by Carasso **[13]**, including the cases with a hyperbolic approximation, cf. (70), and central difference as well as the forward difference approximation of $\frac{\partial}{\partial t}$.

The magnitudes of the elements of the corresponding $\mathbf{D}$-matrix are depicted in Figure 3.13, showing a structure close to the banded one arising from the previously discussed conventional finite-difference approximations.

3.5. Solution procedure. Consider the sampled measurement data

$$\begin{bmatrix} \mathbf{v} \\ \mathbf{v}_x \end{bmatrix}(0) = \left[\begin{array}{c} \mathbf{g} \\ \hline \mathbf{h} \end{array}\right] = \left[\begin{array}{c} [g(0)\ g(\Delta t)\ \ldots\ g(N\Delta t)]^T \\ \hline [h(0)\ h(\Delta t)\ \ldots\ h(N\Delta t)]^T \end{array}\right] . \tag{139}$$

can be used for integration of (133) to obtain the transposed vector containing the discrete solution profile up until the final time $N\Delta t$

$$\mathbf{v}(x) = [v(x,0)\ v(x,\Delta t)\ \ldots\ v(x,N\Delta t)]^T\ ,\quad 0 \le x \le s(t), \tag{140}$$

Direct numerical integration yields solution trajectories (functions of time in vector form) at positions $0 < x \le s(t)$. When an element of the solution vector reaches the boundary condition $v(s(t), t) = f(t)$, cf. (132) this element is excluded and the time interval split into two subintervals for which the computation is repeated. To obtain the boundary position at the element, record the integration distance. In practice, a small number of such interval divisions are necessary to satisfy the boundary condition for a sufficient number of nodes. For each subinterval, starting point and endpoint conditions are not known (except for the first interval starting point, specified by the initial condition at $t = 0$). Therefore, it is reasonable to assume

that the solution extends smoothly across these points and to introduce a corresponding linear extrapolation [**20**] into the difference scheme, expressed by the coefficients $(a_n)_{n=-N}^{N}$, given by the entries of the corresponding row in the **D**-matrix.

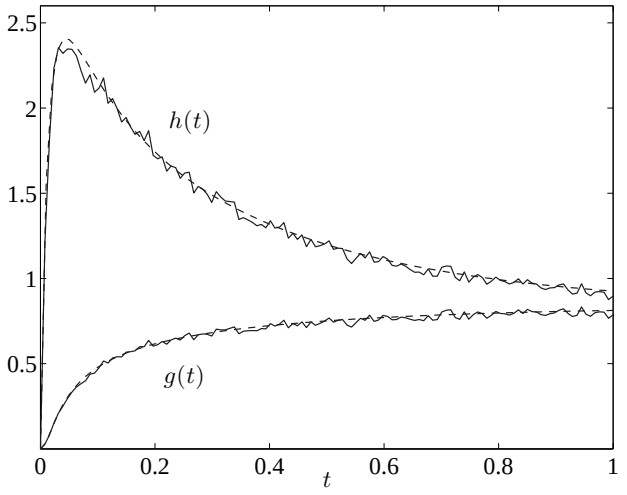

FIGURE 3.14. The field $g(t)$ and flux $h(t)$ at the left end of the geometry in the boundary estimation problem from /**III**/ as functions of time t. The trajectory to be estimated based on these is the constant case $s(t) = 0.2$. The dashed lines depict noiseless signals.

3.6. Computational examples. To get an idea of the performance of the bounded approximation in boundary estimation, we discuss a few computational examples of which the first two have been considered in /**III**/ with a conventional finite-difference approximation to $\frac{\partial}{\partial t}$ and the rest are applications of the bounded approximation described above. All examples are computed using input superposed with stochastic noise of a relative amplitude equal to 1%, however, the results from /**III**/, which were stable but exhibited an offset from the theoretical solution, have been smoothed using polynomial approximation for the final result, i.e., the boundary trajectory $s(t)$. All examples have boundary state $f(t) = 1$ and zero initial state and the input data are computed by solving the corresponding forward problem with known boundary trajectory $s(t)$. In the inverse computations treated in /**III**/, the time step was $\Delta t = 2^{-5}$ and the integration step was $\Delta x = 10^{-5}$. In the other examples the corresponding parameters used were $\Delta t = 2^{-7}$ and $\Delta x = 10^{-5}$, unless otherwise specified. In these direct and inverse computations, the discretizations of the field $v(x, t)$ were different in order to prevent a phenomenon customarily termed "inverse crime", where results of the inverse solution are deceptively good due to the fact that the discretization equals the one used in the solution of the direct problem when generating the input data for the inverse problem.

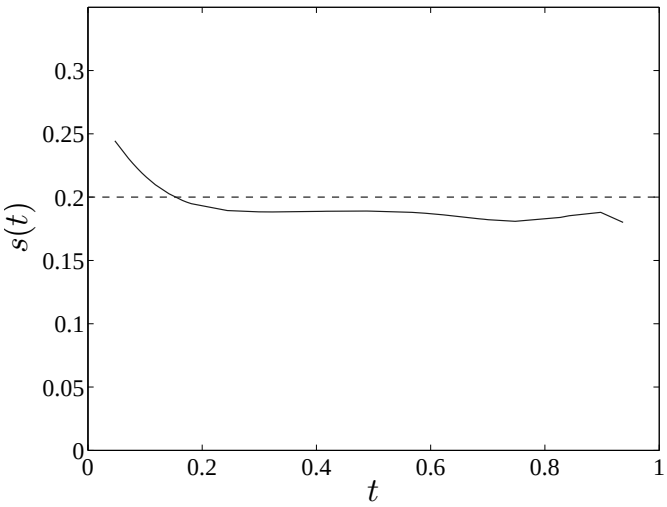

FIGURE 3.15. The estimated boundary trajectory for the constant trajectory case in /**III**/, with theoretical value $s(t) = 0.2$ (dashed), after smoothing by polynomial interpolation.

EXAMPLE 5. This example with a constant boundary trajectory, $s(t) = 0.2$, was considered in /**III**/, by application of a standard four-step forward finite-difference approximation to the operator $\frac{\partial}{\partial t}$. The input data are shown in Figure 3.14 and the smoothed final result, together with the theoretical trajectory, in Figure 3.15. The initial and final portions of the solution were cut out due to offset and oscillation arising from the fact that the peak in the initial flux $h(t)$ and the unknown endpoint condition $v(x, 1)$ make the computations for these portions of the solution computationally unreliable. For most of the time interval of interest, though, the resulting solution is a reasonably good approximation of the "real" theoretical function $s(t)$.

EXAMPLE 6. Also this example with an increasing and oscillating boundary trajectory was considered in /**III**/, by application of a standard four-step forward finite-difference approximation to the operator $\frac{\partial}{\partial t}$. The input data are shown in Figure 3.16 and the smoothed final result, together with the theoretical trajectory, in Figure 3.17. The initial portion of the solution was cut out for the same reason as in the previous example. Here, as in the previous example, an endpoint condition $v(x, 1)$ is not known. We see in the final solution reasonably correct dynamics, however, an increasing lag offset from the theoretical function $s(t)$. Subsequent investigation has shown that this lag is apparently caused by our approximation to the operator $\frac{\partial}{\partial t}$, as using the more accurate **D**-matrix depicted in Figure 3.13 for the bounded approximation described above alleviated the lag offset as demonstrated in the following examples.

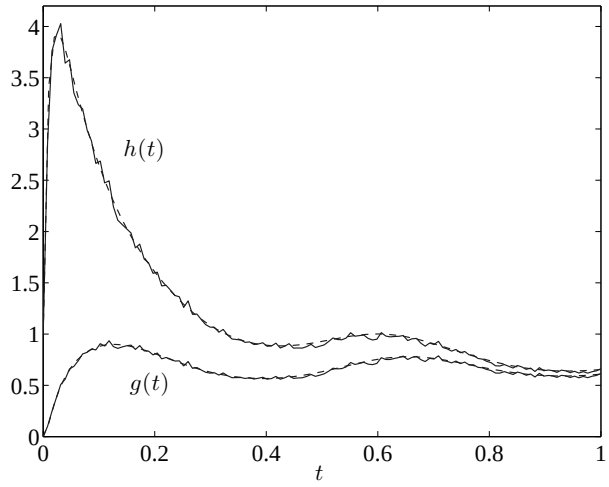

FIGURE 3.16. The field $g(t)$ and flux $h(t)$ at the left end of the geometry in the boundary estimation problem as functions of time t. The trajectory to be estimated based on these is oscillating and increasing. The dashed lines depict noiseless signals.

EXAMPLE 7. Similar to example 5, though not identical due to slight differences in parametrization of the boundary trajectory, (compare Figures 3.14 and 3.18) this example involves use of the **D**-matrix developed in conjunction with the bounded approximation. The field $g(t)$ and flux $h(t)$ are depicted in Figure 3.18 and the estimation result in Figure 3.19. As in the previous examples, initial and final portions of the solution were cut out for the same reasons. Here, quality of the solution for the estimated boundary trajectory is comparable to that of Figure 3.15 in example 5, with perhaps a more correct average than there.

EXAMPLE 8. This example illustrates the advantages of the bounded approximation in comparison with the approach in /**III**/; the result is stable and in phase with the theoretical boundary trajectory, although some minor deviations can be observed. The field $g(t)$ and flux $h(t)$ are depicted in Figure 3.20 and the estimation result in Figure 3.21. When we repeated this computation using a four-point forward approximation like the one in examples 5 and 6 we got a result with the same flaws as in Figure 3.17 of example 6, i.e., a legible lag in the dynamics in addition to other deviations.

EXAMPLE 9. Similar to example 6, though not identical due to slight differences in parametrization of the boundary trajectory, (compare Figures 3.16 and 3.22) this example as well demonstrates the advantage of the bounded approximation. The field $g(t)$ and flux $h(t)$ are depicted in Figure 3.22 and the estimation result in Figure 3.23. Quality of the solution

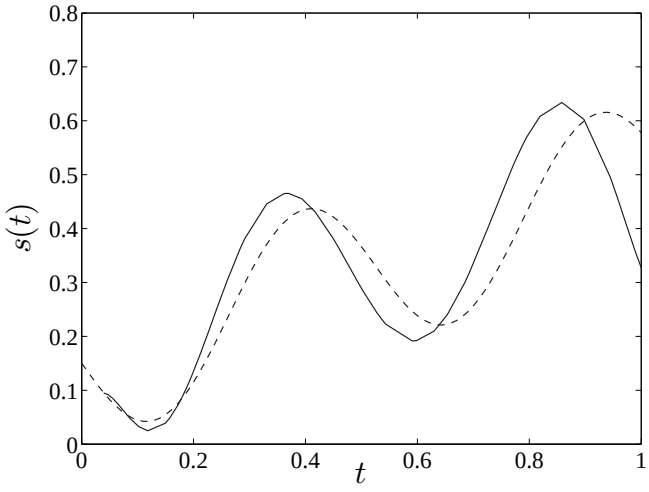

FIGURE 3.17. The estimated boundary trajectory (full line) for the oscillating and increasing trajectory case in /**III**/, after smoothing by polynomial interpolation.

for the estimated boundary trajectory in Figure 3.23 is clearly better than that of Figure 3.17 in example 6.

EXAMPLE 10. In our final example, we challenge the boundary identification method by attempting to estimate a non-differentiable boundary trajectory containing singular points. The field $g(t)$ and flux $h(t)$ are depicted in Figure 3.24 and the estimation result in Figure 3.25. Such trajectories are of interest to us since they frequently occur in the applications treated in /**I-IX**/. An event typically modeled by such a boundary trajectory involves portions of a solid wall "falling off" as a result of mechanical abrasion or erosion. Although not designed for singular trajectory functions, the method still performs reasonably yielding an estimation result reflecting the general features of the theoretical boundary trajectory, as seen from Figure 3.25.

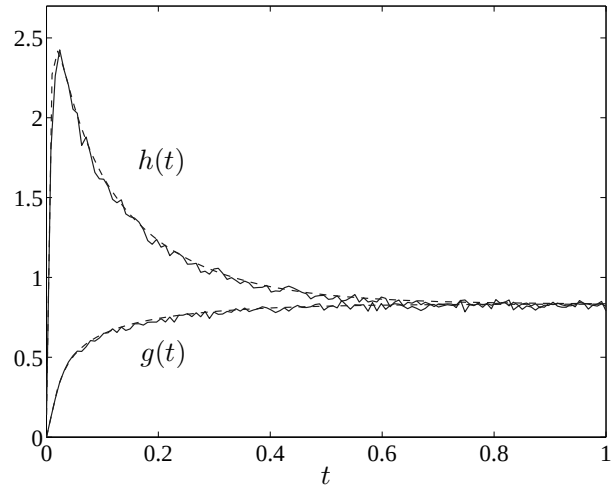

FIGURE 3.18. The field $g(t)$ and flux $h(t)$ at the left end of the geometry in the boundary estimation problem where the trajectory to be estimated based on these is the constant case $s(t) = 0.2$. The dashed lines depict noiseless signals.

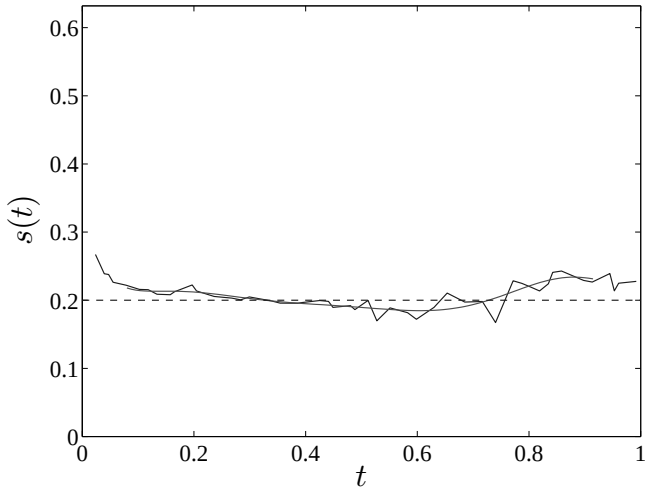

FIGURE 3.19. The estimated boundary trajectory for the constant trajectory case using the bounded approximation, with theoretical value $s(t) = 0.2$ (dashed), shown before and after smoothing by polynomial interpolation.

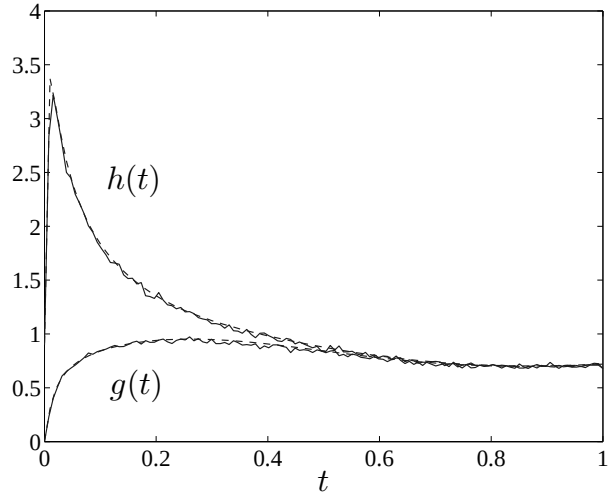

FIGURE 3.20. The field $g(t)$ and flux $h(t)$ at the left end of the geometry in the boundary estimation problem for a trajectory to be estimated based on these which is mainly increasing. The dashed lines depict noiseless signals.

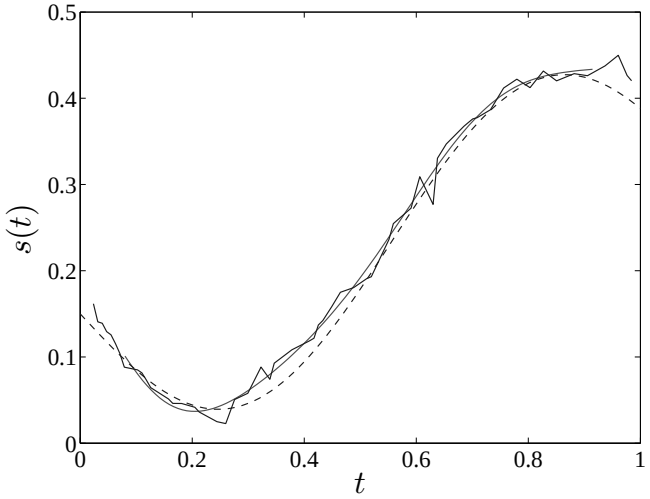

FIGURE 3.21. The estimated boundary trajectory for the mainly increasing trajectory case, using the bounded approximation, before and after smoothing by polynomial interpolation (full lines).

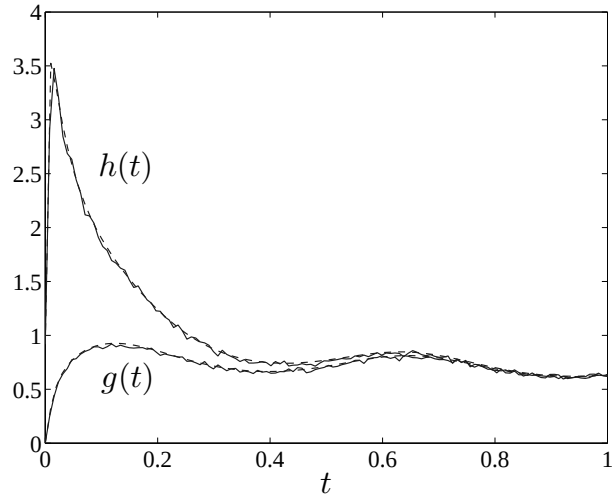

FIGURE 3.22. The field $g(t)$ and flux $h(t)$ at the left end of the geometry in the boundary estimation problem as functions of time t. The trajectory to be estimated based on these is oscillating and increasing. The dashed lines depict noiseless signals.

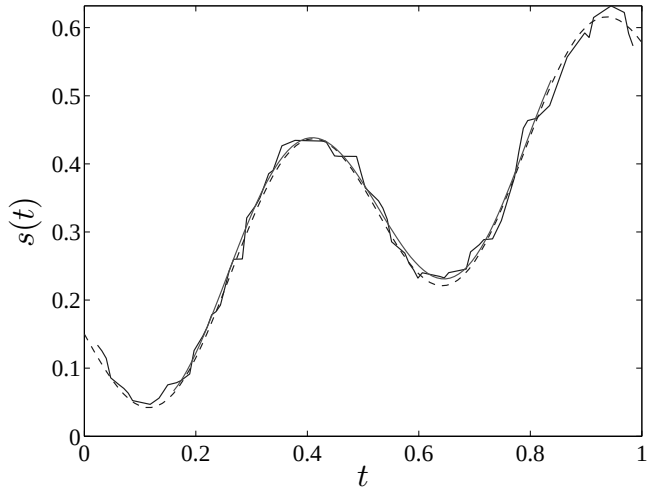

FIGURE 3.23. The estimated boundary trajectory for the oscillating and increasing trajectory case using the bounded approximation, before and after smoothing by polynomial interpolation (full lines).

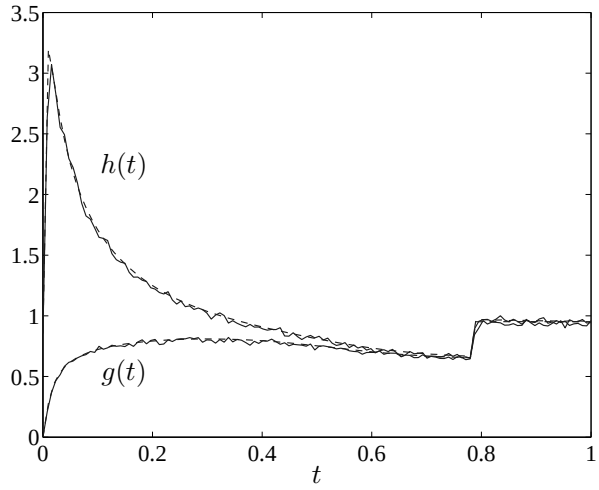

FIGURE 3.24. The field $g(t)$ and flux $h(t)$ at the left end of the geometry in the boundary estimation problem as functions of time t. The trajectory to be estimated based on these is increasing with an abrupt thickness "break down". The dashed lines depict noiseless signals.

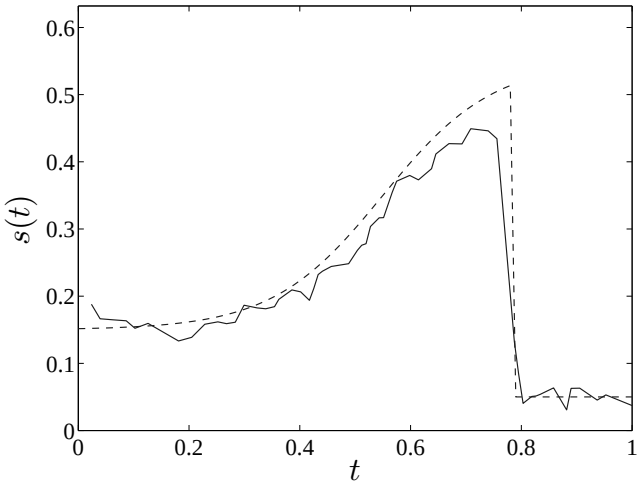

FIGURE 3.25. The estimated boundary trajectory (full line) for the increasing and "breaking down" trajectory case using the bounded approximation. Smoothing was not applied since the boundary trajectory contains singular points.

3.7. Further comments on example results. We now consider (133, 135) as a conventional initial-value problem, which has the unique solution

$$\left[\begin{array}{c} \mathbf{v} \\ \mathbf{v}_x \end{array} \right](x) \quad = \quad \mathrm{e}^{\mathbf{A}x} \left[\begin{array}{c} \mathbf{g} \\ \mathbf{h} \end{array} \right] \ , \tag{141}$$

with the matrix

$$\mathbf{A} = \left[\begin{array}{c|c} \mathbf{0} & \mathbf{I} \\ \hline \mathbf{D} & \mathbf{0} \end{array} \right] \ . \tag{142}$$

The properties of the matrix exponential $\mathrm{e}^{\mathbf{A}x}$ in (141) now determine how the bounded approximation $\mathbf{D}$ of the operator $\frac{\partial}{\partial t}$ in (142) affect the result when the system (133, 135) is integrated. Hence, we can apply the perturbation theory for the matrix exponential outlined in **[22]**, section 11.3.2., according to which we have the inequality

$$\frac{\|\mathrm{e}^{(\mathbf{A}+\mathbf{E})x} - \mathrm{e}^{\mathbf{A}x}\|_2}{\|\mathrm{e}^{\mathbf{A}x}\|_2} \lesssim x\|\mathbf{E}\|_2 \ , \tag{143}$$

where the matrix $\mathbf{E}$ now can be regarded as the difference between two bounded approximations of the operator $\frac{\partial}{\partial t}$. Thus, (143) explains the impact of the approximation on the final identified boundary trajectory as well as the role played by the integration distance x. Our observations in the computational examples also conform to this result.

3.8. Viewpoints on error analysis. As previously noted for the sideways heat conduction equation, e.g. in conjunction with mollification and equation (69), the total computational error can be split up into the *propagated data error*, arising from noise in input data and the *regularization error*, resulting from application of a regularization strategy. Detailed discussions of these, considering the sideways heat equation, can be found in **[2, 3]**. From the standpoint of boundary identification, these two main error types based on the assumed data, i.e., $g(t), h(t) \in L_2(0,\infty)$, can be regarded in a unified analysis if we consider the problem in a transform space as in (114,115) and "cut off" the data so that we are in fact dealing with $\mathtt{G}(\mathsf{p}), \mathtt{H}(\mathsf{p}) \in L_2(0, \mathsf{p_c})$. For simplicity, we study the identification of a constant boundary function $s(t) \equiv \mathtt{s}$, illustrating the ill-posed character of the problem present also for possible variation in the boundary function. Note that an arbitrary boundary function always can be split up into piecewise constant portions to the desired accuracy.

Consider now the problem (110, 111) in the geometry $x \in [0, \mathtt{s}]$ (instead of $x \in [0, 1]$). In the transform space, we are thus dealing with an analogue to (114,115) with a solution similar to (116), relating $\mathtt{F}(\mathsf{p}), \mathtt{G}(\mathsf{p}), \mathtt{H}(\mathsf{p}) \in L_2(0,\infty)$ of the functions $f(t), g(t), h(t) \in L_2(0,\infty)$, looking like

$$\mathsf{G}(\mathsf{p}) = \mathtt{F}(\mathsf{p}) \frac{\mathrm{e}^{0\cdot\sqrt{\mathsf{p}}} + \mathrm{e}^{-0\cdot\sqrt{\mathsf{p}}}}{\mathrm{e}^{\mathtt{s}\sqrt{\mathsf{p}}} + \mathrm{e}^{-\mathtt{s}\sqrt{\mathsf{p}}}} + \frac{\mathtt{H}(\mathsf{p})}{\sqrt{\mathsf{p}}} \ \frac{\mathrm{e}^{-\mathtt{s}\sqrt{\mathsf{p}}} - \mathrm{e}^{\mathtt{s}\sqrt{\mathsf{p}}}}{\mathrm{e}^{\mathtt{s}\sqrt{\mathsf{p}}} + \mathrm{e}^{-\mathtt{s}\sqrt{\mathsf{p}}}} \ , \tag{144}$$

which can be expressed in the form

$$\cosh\left(\mathtt{s}\sqrt{\mathsf{p}}\right)\mathsf{G}(\mathsf{p}) = \mathsf{F}(\mathsf{p}) - \frac{\sinh\left(\mathtt{s}\sqrt{\mathsf{p}}\right)}{\sqrt{\mathsf{p}}}\mathsf{H}(\mathsf{p}) \ . \tag{145}$$

Suppose we have two solutions, $\mathtt{s}_1$ and $\mathtt{s}_2$, to the boundary identification problem for the corresponding input data $\mathsf{G}_1(\mathsf{p})$, $\mathsf{H}_1(\mathsf{p})$ and $\mathsf{G}_2(\mathsf{p})$, $\mathsf{H}_2(\mathsf{p})$, respectively. Note that the known

boundary state $\mathtt{F}(\mathsf{p})$ is identical in these two cases. Hence, stating (145) for the two solutions and subtracting, we obtain

$$\begin{aligned}\cosh(\mathtt{s}_1\sqrt{\mathsf{p}})\mathsf{G}_1(\mathsf{p}) - \cosh(\mathtt{s}_2\sqrt{\mathsf{p}})\mathsf{G}_2(\mathsf{p}) = \\ \tfrac{\sinh(\mathtt{s}_2\sqrt{\mathsf{p}})}{\sqrt{\mathsf{p}}}\mathsf{H}_2(\mathsf{p}) - \tfrac{\sinh(\mathtt{s}_1\sqrt{\mathsf{p}})}{\sqrt{\mathsf{p}}}\mathsf{H}_1(\mathsf{p})\ .\end{aligned} \tag{146}$$

Rearrangement yields

$$\begin{aligned}\left[\cosh(\mathtt{s}_1\sqrt{\mathsf{p}}) - \cosh(\mathtt{s}_2\sqrt{\mathsf{p}})\right]\mathsf{G}_1(\mathsf{p}) + \left[\tfrac{\sinh(\mathtt{s}_1\sqrt{\mathsf{p}})}{\sqrt{\mathsf{p}}} - \tfrac{\sinh(\mathtt{s}_2\sqrt{\mathsf{p}})}{\sqrt{\mathsf{p}}}\right]\mathsf{H}_1(\mathsf{p}) = \\ \cosh(\mathtt{s}_2\sqrt{\mathsf{p}})\left(\mathsf{G}_2(\mathsf{p}) - \mathsf{G}_1(\mathsf{p})\right) + \tfrac{\sinh(\mathtt{s}_2\sqrt{\mathsf{p}})}{\sqrt{\mathsf{p}}}\left(\mathsf{H}_2(\mathsf{p}) - \mathsf{H}_1(\mathsf{p})\right)\ .\end{aligned} \tag{147}$$

Now, applying a standard mean value Theorem, with $\mathtt{s}_s, \mathtt{s}_c \in [\mathtt{s}_1, \mathtt{s}_2]$, on the expressions inside the brackets on the left hand side of (147), we obtain a relationship between differences in input data and the resulting difference in the final solution:

$$\begin{aligned}(\mathtt{s}_1 - \mathtt{s}_2)\left[\sqrt{\mathsf{p}}\sinh(\mathtt{s}_s\sqrt{\mathsf{p}})\mathsf{G}_1(\mathsf{p}) + \cosh(\mathtt{s}_c\sqrt{\mathsf{p}})\mathsf{H}_1(\mathsf{p})\right] = \\ \cosh(\mathtt{s}_2\sqrt{\mathsf{p}})\left(\mathsf{G}_2(\mathsf{p}) - \mathsf{G}_1(\mathsf{p})\right) + \tfrac{\sinh(\mathtt{s}_2\sqrt{\mathsf{p}})}{\sqrt{\mathsf{p}}}\left(\mathsf{H}_2(\mathsf{p}) - \mathsf{H}_1(\mathsf{p})\right)\ .\end{aligned} \tag{148}$$

Denote now

$$\begin{aligned}\mathcal{K}_\mathsf{G}(\mathsf{p}) &= \tfrac{\cosh(\mathtt{s}_2\sqrt{\mathsf{p}})}{\sqrt{\mathsf{p}}\sinh(\mathtt{s}_s\sqrt{\mathsf{p}})\mathsf{G}_1(\mathsf{p}) + \cosh(\mathtt{s}_c\sqrt{\mathsf{p}})\mathsf{H}_1(\mathsf{p})}\ , \\ \mathcal{K}_\mathsf{H}(\mathsf{p}) &= \tfrac{\sinh(\mathtt{s}_2\sqrt{\mathsf{p}})}{\sqrt{\mathsf{p}}\left(\sqrt{\mathsf{p}}\sinh(\mathtt{s}_s\sqrt{\mathsf{p}})\mathsf{G}_1(\mathsf{p}) + \cosh(\mathtt{s}_c\sqrt{\mathsf{p}})\mathsf{H}_1(\mathsf{p})\right)}\ .\end{aligned} \tag{149}$$

Then, applying the triangle inequality yields the error in the boundary estimate, with norms in $L_2(0, \mathsf{p_c})$, according to

$$\|\mathtt{s}_1 - \mathtt{s}_2\|_{L_2} \le \sup_{\mathsf{p}}|\mathcal{K}_\mathsf{G}|\,\|\mathsf{G}_1 - \mathsf{G}_2\|_{L_2} + \sup_{\mathsf{p}}|\mathcal{K}_\mathsf{H}|\,\|\mathsf{H}_1 - \mathsf{H}_2\|_{L_2}\ , \tag{150}$$

Here, introducing the "cutoff-value" $\mathsf{p_c}$ is a strategy for obtaining bounds in absolute value of $\mathcal{K}_\mathsf{G}$ and $\mathcal{K}_\mathsf{H}$. Without applying this limitation, it can be seen from (149) that $\mathtt{s}_2$ being larger than $\mathtt{s}_1$, $\mathtt{s}_s$ and $\mathtt{s}_c$ the numerators in (149) will grow slightly faster than the denominators and make the absolute values $|\mathcal{K}_\mathsf{G}|$, $|\mathcal{K}_\mathsf{H}|$ blow up. In fact, there appears to be an optimal choice of $\mathsf{p_c}$, giving minima for these absolute values. Hence, this strategy of achieving a minimal error bound for the solution can be viewed as a method of regularization similar to the scheme for approximation of the time differentiation operator described above. The Figure 3.26 schematically illustrates this fact for constant $\mathsf{G}_1(\mathsf{p})$ and $\mathsf{H}_1(\mathsf{p})$.

The qualitative features of (150) and Figure 3.26 agree with our computational observations. If the data $g(t), h(t)$ contain high-frequency noise, performance in finding the correct boundary trajectory breaks down through the rapid noise contamination. On the other hand, if the data are smooth, the ill-posedness of the computation does not appear to affect the result considerably.

4. Further development of the boundary identification method

A number of possible areas of further development of the boundary identification method outlined in this chapter can be considered. Many suggestions stem from the applications in /**I-IX**/, like dealing with discontinuous and/or solution dependent coefficients in the governing partial differential equation and boundary conditions. An in-depth look at the numerical properties of the solution of the system of ODE's (133, 135), particularly with respect to the

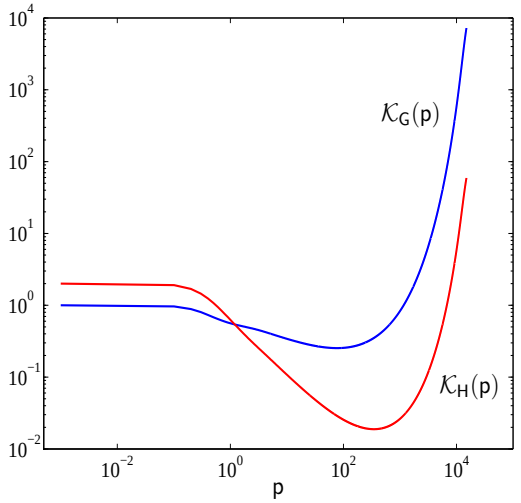

FIGURE 3.26. Schematical behavior of the factors $\mathcal{K}_{\mathsf{G}}$ and $\mathcal{K}_{\mathsf{H}}$ in the error estimate (150), for $\mathsf{G}_1(\mathsf{p}) = 1 = \mathsf{H}_1(\mathsf{p})$ and $\mathtt{s}_1 = 1.8$, $\mathtt{s}_2 = 2$, $\mathtt{s}_c = 1.9$ and $\mathtt{s}_s = 1.85$.

effect of error in the boundary conditions, might also be motivated. In what follows, we will try to suggest strategies for these further areas of development.

4.1. The finite time domain and how this affects intrinsic error propagation. In conjunction with (133), we observed that the finite time domain in principle requires knowledge of the solution for different spatial positions at the final time. There are different approaches to dealing with this difficulty, i.e., extrapolating the solution from neighboring nodes of the vector [**20**] or splitting up the solution into different time windows for which solutions are obtained separately [**2**]. Regardless of the approach, it would be practical to see how the errors hence introduced in the border-column values of the **D**-matrix in (133) affect the error in the estimated boundary trajectory.

4.2. Temperature dependent thermal properties - solution dependent coefficients. When attempting boundary identification from measurements on heat conduction in a solid material, with material properties depending on temperature, we can consider the formulation (c.f. (131, 132))

$$\left[\begin{array}{c} v(t) \\ \kappa(v)v_x(t) \end{array}\right]_x (x) = \left[\begin{array}{cc} 0 & \kappa(v)^{-1} \\ C_p(v)\frac{\partial}{\partial t} & 0 \end{array}\right] \left[\begin{array}{c} v(t) \\ \kappa(v)v_x(t) \end{array}\right] (x) \tag{151}$$

with the "initial" condition and known state at $t = 0$ and on the boundary, according to

$$\begin{gathered} \begin{bmatrix} v(t) \\ \kappa(v)v_x(t) \end{bmatrix}(0) = \begin{bmatrix} g(t) \\ h(t) \end{bmatrix} , \\ v(s(t),t) = f(t) \ , \quad v(x,0) = 0 \ , \\ x \in [0, s(t)], \quad t \in [0, t_f], \ . \end{gathered} \tag{152}$$

Here, $\kappa(v)$ is the thermal conductivity and $C_p(v)$ can be regarded as an effective heat capacity, i.e., a characterization of the ability of the material to store heat energy. The equations of the system (151, 152) have now become nonlinear, but this is no significant complication since an explicit solution method has been shown to work satisfactorily for these problems. See, e.g., **[3]**. Consequently, it is not difficult to modify the method in this chapter to work in applications exhibiting variation in material properties.

4.3. Composite media - discontinuous coefficients. A somewhat related situation, influencing material properties as well, arises in the case of composite media. Then, we have different material properties for different intervals for the x-coordinate. Here, we will assume that these intervals are known to sufficient accuracy, which means that we have a problem with discontinuities in the coefficients of the governing PDE and BC's. As a first approach, we could consider a simple, heuristic approach based on keeping track of the material thicknesses while proceeding with the integration of the system and comparing these to the position of the identified boundary. A more systematic approach to the mathematical characteristics of a problem with discontinuous coefficients might be motivated, however. The risk of ending up with a final solution inside the wrong interval (material layer) would also have to be investigated. Keeping in mind that many applications have both nonlinear and discontinuous coefficients, a combination of these two situations would be worth studying.

CHAPTER 4

Conclusions

Previous work in the metals processing industry, with applications of boundary identification in the domain of PDE's /**I-IX**/, has inspired this study. Investigations of high-temperature processes involving furnaces used for converting iron ore into raw metal and for refining certain metal qualities have made it evident that substantial economical savings and safety improvements are achieved if wear and equipment failure risks can be assessed without shutting down processes. Then, safety margins can be narrowed and maintenance intervals extended for high-temperature industrial equipment, without increasing the risk of failure and/or casualties. This is possible with an effective and reliable boundary identification method, ideally based on monitoring some indirectly influenced variable which is routinely measured or can be measured at a low cost. Furnace wall temperature at different positions is such a variable, suitable as input for a boundary identification method assessing the instantaneous lining wall thickness of the furnace.

We give a background and motivation for the choice of a spatially one-dimensional dynamical model for the boundary, by briefly considering the limitations of spatially two-dimensional models. Dynamics being more important for our applications than adding a spatial dimension and the advantages of the simplest formulation in possible industrial use made us choose the model formulation described in the latter parts of this work. The sideways heat equation is a related topic with many characteristics carrying over to boundary identification, which is why we considered solution properties, noise contamination, regularization and ill-posedness more generally for the sideways heat equation. For boundary identification we study a set of three different methods of estimating the boundary position, of which the two first ones have been developed from a purely mathematical standpoint [**50**] and the third one from a more applied background /**I-IX**/. These methods have different characteristics with benefits and disadvantages. For the mathematically based methods we observed good accuracy and low computation cost, however, with low flexibility for dealing with nonlinear coefficients in the governing PDE. For the third, more applied, method, accuracy suffered from the ill-posedness of the more flexible formulation allowing (at least in principle) nonlinear and discontinuous coefficients in the governing PDE. Finally, we attempted to derive an error estimate, which was observed to conform with our experience from computational trials with the method.

We feel that the present study is a good starting point as a mathematical basis for developing industrial applications of boundary identification, particularly toward dealing with real, nonlinear and discontinuous, material properties and sudden changes due to material "fall-off". With the methods outlined here, it seems feasible to obtain a robust, rapid and sufficiently accurate method using a reasonable amount of mathematical machinery.

Bibliography

[1] D. D. Ang and R. Gorenflo. *Optimal Control of Partial Differential Equations*, chapter "A Nonlinear Abel Integral Equation", pages 26–37. Springer, Berlin/Heidelberg, 1991.

[2] F. Berntsson. *Numerical Solution of an Inverse Heat Conduction Problem.* Licentiate thesis, Linköping Studies in Science and Technology. No. 732., Linköpings Universitet, Department of Mathematics, Linköping, Sweden, 1998.

[3] F. Berntsson. *Numerical Methods for Inverse Heat Conduction Problems.* Dissertation, Linköping Studies in Science and Technology. No. 723., Linköpings Universitet, Department of Mathematics, Linköping, Sweden, 2001.

[4] K. Bryan and L. F. Caudill Jr. Stability and resolution in thermal imaging. In *Proceedings of the Symposium on Parameter Estimation at the 15th ASME Biennial Conference on Vibration and Noise*, Boston, 1995. ASME.

[5] K. Bryan and L. F. Caudill Jr. An inverse problem in thermal imaging. *SIAM Journal of Applied Mathematics*, 59:715–735, 1996.

[6] K. Bryan and L. F. Caudill Jr. Uniqueness for a boundary identification problem in thermal imaging. *Electronic Journal of Differential Equations*, C-1:23–39, 1997.

[7] K. Bryan and L. F. Caudill Jr. Stability and reconstruction for an inverse problem for the heat equation. *Inverse Problems*, 14:1429–1453, 1998.

[8] K. Bryan and L. F. Caudill Jr. Reconstruction of an unknown boundary portion from cauchy data in n-dimensions. *Inverse Problems*, 21:239–256, 2005.

[9] J. R. Cannon. Determination of an unknown coefficient in a parabolic differential equation. *Duke Mathematical Journal*, 30:313–324, 1963.

[10] J. R. Cannon. *The One-Dimensional Heat Equation*, volume 23 of *Encyclopedia of Mathematics and its Applications.* Addison-Wesley, Menlo Park, CA, 1984.

[11] J. R. Cannon and W. Rundell. Recovering a time-dependent coefficient in a parabolic differential equation. *Journal of Mathematical Analysis and Applications*, 160(2):572–582, September 1991.

[12] A. S. Carasso. Determining surface temperature from interior observations. *SIAM Journal of Applied Mathematics*, 42(3):558–574, 1982.

[13] A. S. Carasso. Space marching difference schemes in the nonlinear inverse heat conduction problem. *Inverse Problems*, (8):25–43, 1992.

[14] A. S. Carasso. Slowly divergent space marching schemes in the inverse heat conduction problem. *Numerical Heat Transfer, Part B*, (23):111–126, 1993.

[15] A. S. Carasso. Overcoming Hölder continuity in ill-posed continuation problems. *SIAM Journal of Numerical Analysis*, 31(6):1535–1557, 1994.

[16] A. S. Carasso. Logarithmic convexity and the "slow evolution" constraint in ill-posed initial value problems. *SIAM Journal of Mathematical Analysis*, 30(3):479–496, 1999.

[17] L. Eldén. Approximations for a Cauchy problem for the heat equation. *Inverse Problems*, 3:263–273, 1987.

[18] L. Eldén. Hyperbolic approximations for a Cauchy problem for the heat equation. *Inverse Problems*, 4:59–70, 1988.

[19] L. Eldén. Numerical solution of the sideways heat equation by difference approximation in time. *Inverse Problems*, 11:913–923, 1995.

[20] L. Eldén. Solving an inverse heat conduction problem by a "method of lines". *Transactions of the ASME*, 119:406–412, August 1997.

[21] H. W. Engl. Regularization methods for the stable solution of inverse problems. *Surv. Math. Ind.*, (3):71–143, 1993.

[22] G. H. Golub and C. F. Van Loan. *Matrix Computations*. The Johns Hopkins University Press, Baltimore, 3rd edition, 1996.

[23] G. Gripenberg, S.-O. Londen, and O. Staffans. *Volterra Integral and Functional Equations*. Cambridge University Press, Cambridge, 1990.

[24] L. Guo, D. A. Murio, and C. Roth. A mollified space marching finitedifferences algorithm for the inverse heat conduction problem with slab symmetry. *Computers Math. Applic.*, (19):75–89, 1990.

[25] D. N. Hào. A mollification method for ill-posed problems. *Numerische Mathematik*, (68):469–506, 1994.

[26] V. Isakov. *Inverse Problems for Partial Differential Equations*, volume 127 of *Applied Mathematical Sciences*. Springer-Verlag, New York, 1998.

[27] B. F. Jones Jr. *The Determination of a Coefficient in a Parabolic Partial Differential Equation*. Dissertation, Rice University, Houston, TX, April 1961.

[28] T. Kato. *Perturbation Theory for Linear Operators*, volume 132 of *A Series of Comprehensive Studies in Mathematics*. Springer-Verlag, New York, 2nd edition, 1984.

[29] E. Kreyszig. *Introductory Functional Analysis with Applications*. John Wiley & Sons, New York, 1978.

[30] P. K. Lamm. A survey of regularization methods for first-kind Volterra equations. In D. Colton, H. W. Engl, A. Louis, J. R. McLaughlin, and W. Rundell, editors, *Surveys on Solution Methods for Inverse Problems*, pages 53–82, Wien, New York, 2000. Springer.

[31] H. A. Levine. Continuous data dependence, regularization, and a three lines theorem for the heat equation with data in a space like direction. *Ann. Mat. Pura Appl.*, (134):267–286, 1983.

[32] P. Manselli and K. Miller. Calculation of the surface temperature and heat flux on one side of a wall from measurements on the opposite side. *Ann. Mat. Pura Appl.*, (123):161–183, 1980.

[33] P. M. Morse and H. Feshbach. *Methods of Theoretical Physics*. McGraw-Hill Publishing Company, New York, 1953.

[34] D. A. Murio. The mollification method and the numerical solution of an inverse heat conduction problem. *SIAM J. Sci. Stat. Comput.*, 2:17–34, 1981.

[35] D. A. Murio. The mollification method and the numerical solution of the inverse heat conduction problem by finite differences. *Computers Math. Applic.*, (10):1385–1396, 1989.

[36] D. A. Murio and L. Guo. A stable space marching finite differences algorithm for the inverse heat conduction problem with no initial filtering procedure. *Computers Math. Applic.*, (19):35–50, 1990.

[37] D. A. Murio and C. C. Roth. An integral solution for the inverse heat conduction problem after the method of Weber. *Comput. Math. Applic.*, 15(1):39–51, 1988.

[38] A. W. Naylor and G. R. Sell. *Linear Operator Theory in Engineering and Science*, volume 40 of *Applied Mathematical Sciences*. Springer-Verlag, New York, 1982.

[39] A. Pinkus and S. Zafrany. *Fourier Series and Integral Transforms*. Cambridge University Press, Cambridge, 1997.

[40] G. P. M. Poppe and C. M. J. Wijers. ALGORITHM 680 Evaluation of the complex error function. *ACM Transactions on Mathematical Software*, 16(1):47, March 1990.

[41] E. Radmoser and R. Wincor. Determining the inner contour of a furnace from temperature measurements. Technical Report 12, Industrial Mathematics Institute, Johannes Kepler University of Linz, Linz, Austria, 1998.

[42] R. D. Richtmyer and K. W. Morton. *Difference Methods for Initial-Value Problems*. Tracts in Pure and Applied Mathematics. Wiley Interscience, New York, 2nd edition, 1967.

[43] W. Rudin. *Real and Complex Analysis*. McGraw-Hill Publishing Company, New York, 3rd edition, 1986.

[44] I. M. Skaar. *Monitoring the Lining of a Melting Furnace*. Dissertation, Norges Teknisk-Naturvitenskapelige Universitet, Trondheim, Norway, April 2001.

[45] K. Sørli and I. M. Skaar. Monitoring the wear-line of a melting furnace. In *Inverse Problems in Engineering: Theory and Practice. 3rd International Conference on Inverse Problems in Engineering*, pages 1–11, Port Ludlow, WA, June 1999. ASME.

[46] O. J. Staffans. *Well-Posed Linear Systems*. Cambridge University Press, Cambridge, 2005.

[47] L. Tang and J. D. Baeder. Uniformly accurate finite difference schemes for p-refinement. *SIAM J. Sci. Comput.*, 20(3):1115–1131, 1999.

[48] A. N. Tikhonov and A. A. Samarskii. *Equations of Mathematical Physics*. International Series of Monographs in Pure and Applied Mathematics. Pergamon Press, New York, 1963.

[49] C. F. Weber. Analysis and solution of the ill-posed inverse heat conduction problem. *Int. J. Heat Mass Transfer*, 24(11):1783–1792, 1981.

[50] N. Yarlikina and H. Walrath. Determining the length of a one-dimensional bar from thermal measurements. Technical Report MSTR 04-02, Rose-Hulman Institute of Technology, Terre Haute, IN, 2004.